

# Development of strategies for continuous desalination of weak black liquor based on phase-behaviour analysis

Nicholas I. Canabarro<sup>a</sup>, Darius J. Yeadon<sup>a</sup>, Maximilian Wörner<sup>b</sup>, Ursel Hornung<sup>b</sup>, Frédéric Vogel<sup>a,c</sup>, David Baudouin<sup>a,\*</sup>

<sup>a</sup> Laboratory for Sustainable Energy Carriers and Processes (LEP), Paul Scherrer Institute (PSI), Villigen 5232, Switzerland

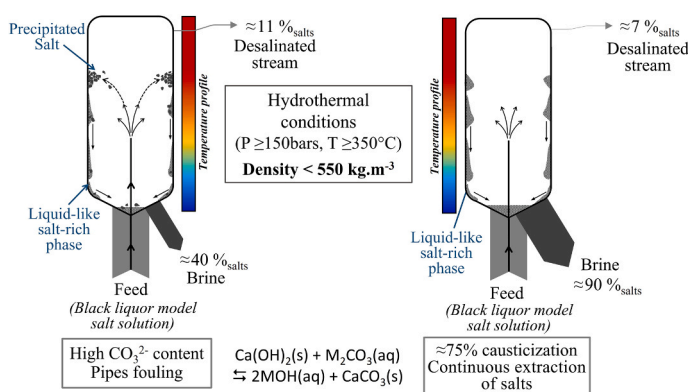
<sup>b</sup> Institut für Katalyseforschung und Technologie (IKFT), Karlsruher Institut für Technologie (KIT), Eggenstein-Leopoldshafen 76344, Germany

<sup>c</sup> Fachhochschule Nordwestschweiz (FHNW), Institut für Biomasse und Ressourceneffizienz, 5210 Windisch, Switzerland

## HIGHLIGHTS

- HP-DSC as a tool for identifying the phase behaviour of salts mixtures from black liquor.
- Type 1 salt behaviour is observed after removing 75% of carbonate from the black liquor model.
- 75% carbonate reduction ensures continuous salt separation, allowing HTL/HTG operation.
- Doubling Type 1 salts prevents clogging, but does not prevent the accumulation of salts.

## GRAPHICAL ABSTRACT



## ARTICLE INFO

### Keywords:

Hydrothermal liquefaction  
Weak black liquor  
Salt separation  
Supercritical water  
Phase behavior

## ABSTRACT

This paper investigated different strategies to prevent salt deposition during weak black liquor (WBL) desalination under hydrothermal liquefaction conditions based on phase behaviour analysis. Phase equilibria of model salt solutions replicating the WBL composition were studied by high-pressure differential scanning calorimetry (HP-DSC) and different strategies to induce the Type 1 salt behaviour were applied. Two strategies led to an optimised salt separation: adjusting the concentrations of Type 1 salts, NaOH and NaHS, present in the WBL, and selectively exchanging carbonate from the model salt solution by replacing it with hydroxide. These strategies were tested in PSI's continuous salt separation test rig, considering the recovering of salts. Although increasing the concentration of the Type 1 salts (NaOH and NaSH) impacted the precipitation temperature and extent of the

**Abbreviations:** SCW, Supercritical water; SCWD, Supercritical water desalination; HTL, Hydrothermal liquefaction; WBL, Weak black liquor; VLE, Vapour-liquid equilibrium; VSE, Fluid-solid equilibrium; HP-DSC, High pressure differential scanning calorimetry; SNG, Synthetic natural gas;  $\dot{m}_{\text{Brine}}^{\text{ion}}$ , mass flow rate of the ion in the brine;  $\dot{m}_{\text{Desalinated stream}}^{\text{ion}}$ , mass flow rate of the ion in the desalinated stream;  $\dot{m}_{\text{Feed}}^{\text{ion}}$ , mass flow rate of the ion in the feed;  $\dot{m}_{\text{Effluent } x}^{\text{ion}}$ , mass flow rate of an ion in either the brine or the desalinated stream; ICP-OES, Inductively coupled plasma optical emission spectroscopy; TC, Total carbon; TOC, Total organic carbon; TIC, Total inorganic carbon.

\* Corresponding author.

E-mail address: [david.baudouin@psi.ch](mailto:david.baudouin@psi.ch) (D. Baudouin).

<https://doi.org/10.1016/j.supflu.2024.106230>

Received 28 November 2023; Received in revised form 29 February 2024; Accepted 1 March 2024

Available online 2 March 2024

0896-8446/© 2024 The Authors. Published by Elsevier B.V. This is an open access article under the CC BY license (<http://creativecommons.org/licenses/by/4.0/>).

salts, the strategy was not able to prevent it entirely. The HP-DSC results confirmed the efficiency of carbonate replacement by hydroxide since the Type 1 behaviour was observed after exchanging 75% of the carbonate. In the presence of organics, some salt accumulation and overflow into the desalinated stream occurred, which was addressed by optimising the brine flow rate.

## 1. Introduction

The recent increases in the worldwide energy demand [1] have led scientists to look for alternatives to replace fossil fuels with renewable energy sources, looking for options to mitigate concerns related to climate change and promising technologies to improve efficiency through the energy conversion processes [2,3]. The integrated bio-refinery concept is one of the most promising for biomass valorisation into added-value molecules. It uses the by-products from the core process as feedstock for energy conversion to increase the plant's exergy efficiency and reduce greenhouse gas emissions [4,5]. In the specific case of the pulp industry, the fifth-largest industrial energy consumer and accounting for 5% of the whole energy consumed in this sector [6], some actions must be taken to improve energy efficiency, ensure energy security, and decrease the dependency on fossil-sourced chemicals [7].

The predominant process for pulp production, the Kraft process, involves the digestion of woody chips at elevated temperatures (145–170 °C) and pressures (6–7 bar), which plays an essential role in cellulose separation from lignin and hemicellulose [8–10]. In this stage, an aqueous solution called white liquor (15–20 wt% NaHS and NaOH) is brought into contact with the lignocellulosic biomass. The cellulose fibres are separated from the solubilised compounds, the latter constituting a side stream known as weak black liquor (WBL), mainly containing lignin, hemicellulose and inorganic salts [11,12]. Currently, pulp plants reuse the black liquor in boilers to improve energy efficiency and regenerate sodium sulfide. The high amount of water in the WBL is a drawback, and WBL must be concentrated to at least 65% of solids before being forwarded to the boilers [13], an evaporation step that is energy intensive. Besides, the deposition of inorganic salts is also a downside, which might lead to corrosion, and reduce heat transfer and net power generation efficiency [14,15].

Several studies have demonstrated alternatives to WBL valorisation into fuels and chemicals [16], and some have pointed out the capability of converting WBL into bio-crude via hydrothermal liquefaction (HTL) [17,18]. It is a promising technology to convert wet biomass into liquid biofuels without needing additional pre-treatment steps, such as drying, to make it suitable for energy conversion [19]. The HTL process occurs at high temperatures (typically 300–400 °C) and pressures (100–300 bars), near the critical point of water ( $T_c = 374$  °C and  $P_c = 221$  bars), where its properties, such as density and dielectric constant, undergo drastic changes. In supercritical water, even non-polar organics are easily solubilised, while the solubility of inorganic salts is strongly reduced [20,21]. This decrease of salt solubility can present a threat for a continuous process because of fouling or even plugging of pipes. Therefore, developing a reliable strategy to extract the inorganic salts from the mainstream prior to the HTL process has proven crucial [12].

Although it presents negative aspects, the low solubility of salts in supercritical water has been exploited for industrial purposes such as supercritical hydrothermal synthesis (SHS) and supercritical water desalination (SCWD) [22,23]. Under supercritical conditions, the thermodynamics of the salts is complex, and their continuous extraction relies on the nature of the salts in SCW and their interaction with water and other salts [20,21]. Depending on the phase behaviour of the binary salt-water mixture under hydrothermal conditions, the salts can be classified broadly as either Type 1 or Type 2 [24]. Type 1 mixtures exhibit a positive temperature coefficient of solubility (t.c.s), forming a pseudo-vapour-liquid equilibrium (VLE) under supercritical conditions. The liquid-like phase (brine) presents a high concentration of salts and is in equilibrium with a salt-depleted vapour-like phase. On the other

hand, Type 2 mixtures present a change in t.c.s leading to a drop in the solubility of the salts and forming a fluid-solid (VSE) equilibrium. The solids are prone to precipitate, which can cause pipeline blockages and corrosion in the plant facilities [25,26].

The WBL is a complex mixture containing a high concentration of inorganic salts from the unreacted cooking mixture (NaOH and Na<sub>2</sub>S) and by-products formed during digestion (Na<sub>2</sub>SO<sub>4</sub>, Na<sub>2</sub>CO<sub>3</sub>, and Na<sub>2</sub>S<sub>2</sub>O<sub>3</sub>). Similar salts with potassium as a counter cation are also found in WBL composition but in smaller amounts [12,27]. Sodium thiosulfate dissociates into sulfite, sulfide, and sulfate ions in SCW [28], while Na<sub>2</sub>S fully hydrolyses to NaHS even in highly basic media [29]. NaOH and NaHS have been considered Type 1 salts, while Na<sub>2</sub>CO<sub>3</sub> and Na<sub>2</sub>SO<sub>4</sub> are Type 2 salts [12,24]. High pressure differential scanning calorimetry (HP-DSC) is an important tool in the phase behaviour analysis of multi-component salt mixtures in SCW [30]. Reimer and Vogel [31] studied ternary solutions related to biomass for obtaining relevant data for the conversion of wet biomass to synthetic natural gas (SNG) in a SCWG process by HP-DSC. They found that the phase behaviour of ternary hydrothermal salt solutions strongly correlates with the behaviour of the binary boundary subsystems, of which they consist. Research on the phase behaviour of multi-component salt mixtures in SCW has shown that the hydrothermal brine of Type 1 salts might be able to dissolve the precipitated solids of Type 2 salts [32–35]. Voisin et al. [35] investigated the solubility of NaCl (Type 1) in SCW and its influence on the solubility of Na<sub>2</sub>SO<sub>4</sub> (Type 2). They concluded that the high concentration of NaCl in the water brine maintains a high polarity and enables the dissolution of Na<sub>2</sub>SO<sub>4</sub>. Schubert et al. [36] studied the phase behaviour of ternary mixtures in supercritical conditions and showed Na<sub>2</sub>CO<sub>3</sub> and K<sub>2</sub>SO<sub>4</sub>, both Type 2 salts, might behave as Type 1 when mixed at specific conditions. According to the authors, a certain quantity of K<sub>2</sub>CO<sub>3</sub> (Type 1) might be formed in SCW, leading to a salt recovery of up to 95%. Therefore, if the VLE can be established for the multi-component salt mixtures, a supercritical water salt precipitation strategy could be developed to treat a liquid waste stream such as WBL.

In this paper, phase equilibria of model salt solutions replicating that of WBL were studied by HP-DSC to better understand how to influence salt recovery by inducing Type 1 behaviour of salt mixtures under supercritical conditions. Two distinguished strategies to optimise salt precipitation during HTL of WBL were assessed. It included the enrichment of Type 1 salts by doubling the concentration of NaOH and NaHS and the depletion of Type 2 salts by reducing carbonate concentration (by 25, 50, and 75%) in the neat model salt solution. The influence of organic compounds on salt separation efficiency was also assessed by adding sodium and potassium acetates into the inorganic model salt solutions. The most promising strategies were tested in PSI's continuous salt separation test rig considering the overall salt recovery.

## 2. Materials and methods

### 2.1. Inorganic model salt solutions

The complex mixture of WBL undergoes a variety of competing reactions under hydrothermal conditions: hydrolysis, decarboxylation, and condensation/re-polymerisation of organics, as well as salt precipitation. In order to study the behaviour of the salt mixture present in the WBL, a model salt solution containing inorganic salts (MOH, M<sub>2</sub>SO<sub>4</sub>, M<sub>2</sub>CO<sub>3</sub> and MHS, with M = Na or K) was prepared based on the characterisation of the WBL (Table 1). Salt separation was optimised by two methods (Table 2), i) adjusting the concentrations of Type 1 salts, NaOH

**Table 1**

Composition of Black Liquor from hard wood eucalyptus trees.

Parameter	Unit		Value
pH		Slurry	13.31
Conductivity	mS cm <sup>-1</sup>		75.50
Dry matter	wt%		14.50
Ash	wt%		4.92
Inorganic C	wt%		0.18
Organic C	wt%		4.59
Total C	wt%		4.77
CO <sub>3</sub> <sup>2-</sup>	wt%	Dry matter	6.48
Total S	wt%		4.70
SO <sub>4</sub> <sup>2-</sup>	wt%		1.88
HS <sup>-</sup>	wt%		2.11
Total Na	wt%		17.73
Total K	wt%		1.28
Residual HO <sup>-</sup>	wt%		5.35

and NaHS, present in the WBL, and ii) selectively exchanging carbonate for hydroxide in the model salt solution. The model salt solutions allow for a simplified study of the phase equilibria by HP-DSC of the salt mixtures, whilst avoiding interference from side reactions. The presence of organics is known to affect the salt separation efficiencies, due to changes in fluid density and saturation temperature [37]. In order to gain an insight into the effect of organics, metal acetates (M = Na and K) were added (Table 3), as they represent a significant proportion of the organics present in WBL and have shown not to undergo significant degradation in SCW. The organic content in the model salt solutions was calculated based on the remaining Na and K present from the characterisation of the WBL.

Sodium hydroxide (NaOH) from Sigma-Aldrich and sodium sulfide nonahydrate (Na<sub>2</sub>S·9 H<sub>2</sub>O) from Honeywell Fluka were both of a purity equal to or greater than 98%. Sodium hydrosulfide (NaHS·xH<sub>2</sub>O, where x=1.46) was obtained from Sigma-Aldrich. The potassium hydroxide (KOH) pellets, sourced from Sigma-Aldrich, had a purity of 87.86%, with impurities including 1.74 wt% of potassium carbonate (K<sub>2</sub>CO<sub>3</sub>) and water, which were accounted for during solution preparation. Other salts used, including sodium carbonate (Na<sub>2</sub>CO<sub>3</sub>) from Merck, potassium carbonate (K<sub>2</sub>CO<sub>3</sub>) from Sigma-Aldrich, sodium sulfate (Na<sub>2</sub>SO<sub>4</sub>) from Alfa Aesar, sodium acetate trihydrate (NaCH<sub>3</sub>CO<sub>2</sub>) from Fluka and potassium sulfate (K<sub>2</sub>SO<sub>4</sub>) from Sigma-Aldrich, all exhibited a purity of equal to or greater than 99%. Deionised water (DI water) with a conductivity of less than 5 μS cm<sup>-1</sup> was utilised for solution preparation. It is noteworthy that all sulfide salts were stored under nitrogen upon delivery from the supplier to prevent oxidation.

## 2.2. High-pressure differential scanning calorimetry (HP-DSC)

Phase equilibria data of the model salt solutions were obtained by isochoric high-pressure differential scanning calorimetry on a Sensys HP-DSC (SETARAM, France), equipped with a high-precision Calvet-type sensor. Incoloy A-286 crucibles supplied by the manufacturer (inner volume 128.6 ± 0.5 μL [38], as well as in-house made Titanium grade 5 (Ti-6Al-4 V) crucibles (135.4 ± 0.6 μL) were used. The crucibles were filled with 38.6 ± 0.1 mg and 40.6 ± 0.1 mg of model salt solution

**Table 2**

Composition of model salt solutions (wet basis) studied without organics by HP-DSC in experiments A to I; experiment A is based on the characterisation of the WBL described in Table 1.

Salt	Unit	Experiment								
		A	B	C	D	E	F	G	H	I
Na <sup>+</sup>	mol·L <sup>-1</sup>	0.86	1.72	0.86	1.72	0.86	0.86	0.86	0.86	0.88
K <sup>+</sup>	mol·L <sup>-1</sup>	0.04	0.04	0.04	0.04	0.04	0.04	0.04	0.04	0.04
OH <sup>-</sup>	mol·L <sup>-1</sup>	0.43	0.86	0.43	0.86	0.43	0.43	0.52	0.61	0.69
HS <sup>-</sup>	mol·L <sup>-1</sup>	0.09	0.09	0.18	0.18	0.09	0.09	0.09	0.09	0.09
SO <sub>4</sub> <sup>2-</sup>	mol·L <sup>-1</sup>	0.03	0.03	0.03	0.03	0.03	0.03	0.03	0.03	0.03
CO <sub>3</sub> <sup>2-</sup>	mol·L <sup>-1</sup>	0.14	0.14	0.14	0.14	0.04	0.08	0.11	0.08	0.04

**Table 3**

Composition of model salt solutions (wet basis) studied with organics by HP-DSC in experiments J to P; experiment J is based on the characterisation of the WBL described in Table 1 plus addition of acetates.

Salt	Unit	Experiment						
		J	K	L	M	N	O	P
Na <sup>+</sup>	mol·L <sup>-1</sup>	1.20	1.61	1.20	1.79	1.22	1.21	1.21
K <sup>+</sup>	mol·L <sup>-1</sup>	0.06	0.06	0.06	0.06	0.06	0.06	0.06
OH <sup>-</sup>	mol·L <sup>-1</sup>	0.43	0.88	0.43	0.88	0.52	0.59	0.66
HS <sup>-</sup>	mol·L <sup>-1</sup>	0.09	0.09	0.18	0.21	0.09	0.09	0.09
SO <sub>4</sub> <sup>2-</sup>	mol·L <sup>-1</sup>	0.03	0.03	0.03	0.03	0.03	0.03	0.03
CO <sub>3</sub> <sup>2-</sup>	mol·L <sup>-1</sup>	0.15	0.15	0.15	0.16	0.12	0.08	0.04
CH <sub>3</sub> CO <sub>2</sub>	mol·L <sup>-1</sup>	0.38	0.38	0.38	0.38	0.37	0.38	0.37

for the Incoloy and titanium crucibles, respectively, to achieve a fluid density of 300 ± 1 kg·m<sup>-3</sup> under monophasic conditions. The crucibles were purged with argon to avoid the oxidation of the NaHS and sealed prior to measurements. An empty crucible filled with air at room temperature and 1 bar was used as a reference.

A slow heating and cooling ramp of 0.1 K·min<sup>-1</sup> was used for all measurements, unless stated otherwise, for precise scanning and good peak separation. Phase transitions were analysed using the Calisto software (AKTS, Switzerland), and further information can be found in [30]. The repeatability of the HP-DSC was assessed from measurements with deionised water. The critical temperature was found to be 373.3 ± 0.2 °C, compared to 373.95 °C from the NIST reference database [39], the difference being caused by an overcooling phenomenon [38], and also due to the presence of argon in the headspace. All the data presented in this paper refer to the measured temperature, and no correction was applied.

## 2.3. Continuous salt separation tests

In order to investigate the salt separation efficiency in a continuous process, the most promising strategies assessed by HP-DSC were tested in a continuous salt separation rig, as presented in Table 4.

The salt separation tests were performed on the continuous salt separation test rig Salsan-II [40], as shown in Fig. 1. The separation vessel is made of Zircaloy-2 with an inner diameter of 1.2 cm, an external diameter of 3 cm and a length of 43 cm. The top and bottom fittings and connecting pipes are made of stainless steel 316Ti (SITEC, Switzerland). An HPLC pump (PU-01, Waters) introduces the cold feed into the vessel bottom via a riser tube, whose tip is at 78 mm from the bottom of the vessel. Injection of the feed from the bottom has proven to significantly improve the efficiency of salt separation, as opposed to an injection from the top [41]. Eight independent annular heaters control the vessel temperature. The feed stream splits into two streams inside the vessel, a desalinated stream at the top of the vessel and a salt-rich stream at the bottom, called “brine” herein. The overall salt concentration was monitored in both streams leaving the salt separator, after cooling and depressurisation, by online conductivity meters (WTW Cond 340i), which allowed to assess the overall salt recovery during the experiments. A backpressure regulator (BPR-01, Tescom), mounted

**Table 4**

Details of continuous salt separation experiments performed. For all the experiments, the heaters H-01 to H-04 were set to  $450 \pm 1^\circ\text{C}$ , the heaters H-06 to H-08 to  $400 \pm 1^\circ\text{C}$  (see Fig. 1), and the pressure was  $250 \pm 5$  bars.

Experiment									
Ion	unit	AC <sup>a</sup>	BC	CC	DC	EC	FC	GC	HC
Na <sup>+</sup>	mol·L <sup>-1</sup>	0.86	1.40	0.86	0.86	1.20	1.40	0.86	0.86
K <sup>+</sup>	mol·L <sup>-1</sup>	0.04	0.04	0.04	0.04	0.04	0.04	0.06	0.04
OH <sup>-</sup>	mol·L <sup>-1</sup>	0.43	0.87	0.53	0.67	0.43	0.87	0.67	0.53
HS <sup>-</sup>	mol·L <sup>-1</sup>	0.09	0.21	0.09	0.09	0.09	0.21	0.09	0.09
SO <sub>4</sub> <sup>2-</sup>	mol·L <sup>-1</sup>	0.03	0.03	0.03	0.03	0.03	0.03	0.03	0.03
CO <sub>3</sub> <sup>2-</sup>	mol·L <sup>-1</sup>	0.15	0.15	0.11	0.04	0.15	0.15	0.04	0.11
CH <sub>3</sub> CO <sub>2</sub>	mol·L <sup>-1</sup>	-	-	-	-	0.37	0.37	0.37	0.37
Feed mass flow rate	g·min <sup>-1</sup>	6.39	6.40	6.14	6.25	6.33	6.43	6.31	6.21
Brine mass flow rate	g·min <sup>-1</sup>	1.98	2.03	2.01	1.91	1.27	1.82	1.80	2.52
Feed conduct.	S·cm <sup>-1</sup>	0.11	0.19	0.12	0.15	0.11	0.19	0.15	0.12

<sup>a</sup> Based on black liquor composition of Table 1.

downstream of the cooler in the desalinated stream, controlled the pressure inside the vessel. At the same time, a mass flow controller (MFC-01, Bronkhorst LIQUI-FLOW L29-ABD-11-z-80S coupled to a Bronkhorst EL-FLOW F-033 C-LIU-11-K) regulated the brine mass flow rate. An analytical balance measured the mass decrease of the feed container. Desalinated and brine streams were collected in sealed bottles under N<sub>2</sub> atmosphere, while their masses were measured by two analytical balances. The mass flow rate of all streams was independently checked by a gravimetric method. The temperature was measured by four K-type thermocouples installed at the top/bottom (T-02 and T-03) of the separator and at the outlets (T-01 and T-04), respectively. During the exposure to the model salt solutions at supercritical conditions, the standard commercial 316-sheathed thermocouples experienced fast corrosion, prompting the provision of an in-house made Titanium sheath for the thermocouples T-01- and T-02. Three pressure transducers installed on the feed stream (P-01), bottom stream (P-02) and top stream (P-03), respectively, monitored the pressure. A Labview® programme recorded all temperatures, pressures, conductivities of the outlet streams, and signals of the analytical balances.

The experiments comprised seven main steps, described in the

following: (1) flush the setup at ambient temperature and pressure with DI water (generally overnight) until reaching the DI water conductivity value ( $< 5 \mu\text{S cm}^{-1}$ ); (2) pressurise the setup to 250 bar; (3) heat up the fluids inside the separator to around  $150^\circ\text{C}$ ; (4) set the first four heaters to  $450^\circ\text{C}$ , while the bottom four are set to  $400^\circ\text{C}$ ; (5) wait for steady temperatures; (6) switch feed from water to the salt model solution to start the separation test ( $t = 0$ ); (7) flush the setup with DI water at the same conditions (pressure and temperature) and then proceed to subcritical conditions overnight (ca.  $150^\circ\text{C}$ ). The filters F-01 and F-02 were inspected after each experiment.

Salt separation efficiency and the recovery of each element in each effluent were calculated by Eqs. 1 and 2.

$$\text{Total recovery} = \frac{\dot{m}_{\text{Brine}}^{\text{ion}} + \dot{m}_{\text{Desalinated stream}}^{\text{ion}}}{\dot{m}_{\text{Feed}}^{\text{ion}}} \cdot 100\% \quad (1)$$

$$\text{Recovery} = \frac{\dot{m}_{\text{Effluent } x}^{\text{ion}}}{\dot{m}_{\text{Feed}}^{\text{ion}}} \cdot 100\% \quad (2)$$

where  $\dot{m}_{\text{Brine}}^{\text{ion}}$ ,  $\dot{m}_{\text{Desalinated stream}}^{\text{ion}}$  and  $\dot{m}_{\text{Feed}}^{\text{ion}}$  are the mass flow rates of the

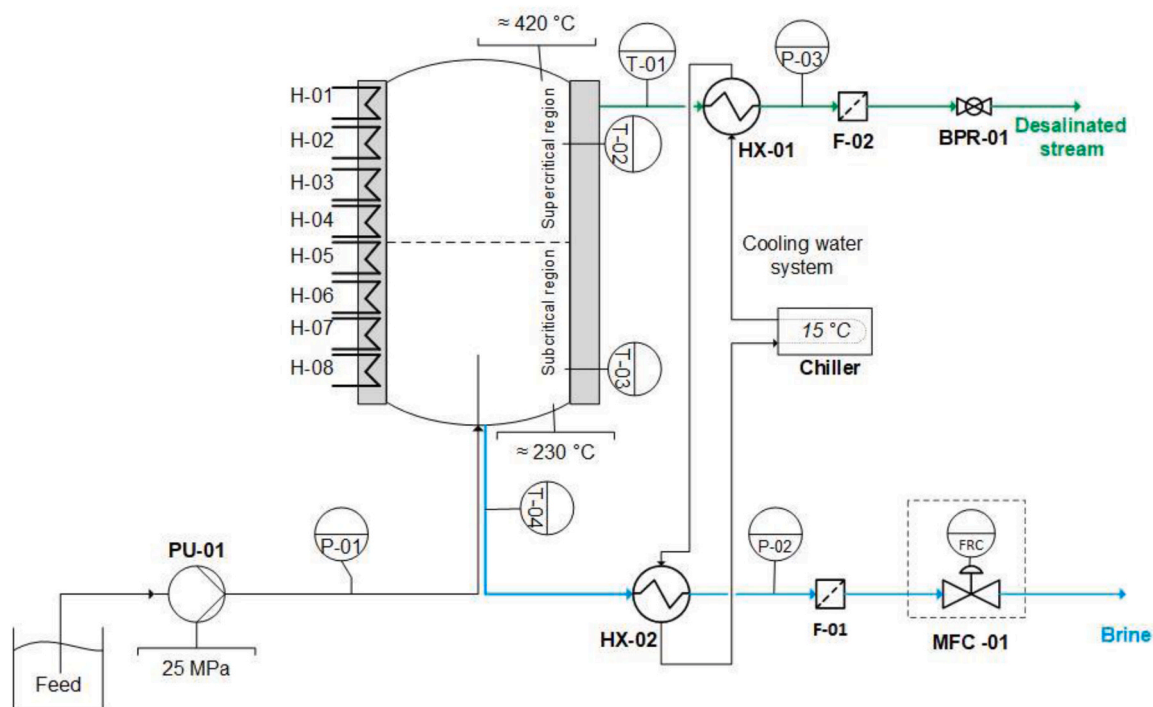


**Fig. 1.** Simplified flow scheme of the continuous salt separator Salsan II. PU-01: HPLC pump; BPR-01: backpressure regulator; F-01 and F-02: filters; MFC-01: mass flow controller; HX-01 and HX-02: heat exchangers; T-01, T-02, T-03 and T-04: thermocouples; P-01, P-02, and P-03: pressure indicators.

**Table 5**

List of chemical species considered in the calculations of potassium and sodium acetates solubility.

Components
<b>Aqueous phase</b>
o $\text{NaCH}_3\text{CO}_2\text{-H}_2\text{O}$ : $\text{Na}^+$ , $\text{CH}_3\text{CO}_2^-$ , $\text{CO}_3^{2-}$ , $\text{NaOH}$ , $\text{CH}_3\text{COOH}$ , $\text{HCO}_3^-$ , $\text{H}^+$ , $\text{OH}^-$ , $\text{H}_2\text{O}$
o $\text{KCH}_3\text{CO}_2\text{-H}_2\text{O}$ : $\text{K}^+$ , $\text{CH}_3\text{CO}_2^-$ , $\text{CO}_3^{2-}$ , $\text{KOH}$ , $\text{CH}_3\text{COOH}$ , $\text{HCO}_3^-$ , $\text{H}^+$ , $\text{OH}^-$ , $\text{H}_2\text{O}$
<b>Solid phases</b>
o $\text{NaCH}_3\text{CO}_2$
o $\text{KCH}_3\text{CO}_2$

ion in the brine, desalinated and feed streams, respectively. The term  $\dot{m}_{\text{Effluent } x}^{\text{ion}}$  stands for the mass flow rate of an ion in either the brine or the desalinated stream.

#### 2.4. Analytical procedures

Inductively coupled plasma optical emission spectroscopy (ICP-OES, Spectroblue SOP, Spectro Analytical Instruments) was used to analyse sodium, potassium and sulphur present in the samples. Volumetrically defined aliquots were weighed to determine the density, and then a large excess of  $\text{H}_2\text{O}_2$  was added to fully oxidise sulfides to sulfate, preventing the production and loss of gaseous  $\text{H}_2\text{S}$  during the preparation of the samples for ICP analysis (acidification with 2.5 wt% nitric acid). For the samples containing organic compounds, aqua regia digestion was applied: around 0.25 g of the sample was treated with 1 mL of concentrated  $\text{HNO}_3$  and 3 mL of concentrated  $\text{HCl}$  in PTFE vials and then heated in a microwave oven for 5 min at 500 W. Then, all the samples were filtered (0.45  $\mu\text{m}$ ), diluted to a concentration between 1 and 100  $\text{mg}\cdot\text{L}^{-1}$  in PE volumetric flasks, and stored in 5 mL PE conical centrifuge tubes until measurement. Calibration was done with standard solutions containing 1, 5, 10, 50, and 100  $\text{mg}\cdot\text{L}^{-1}$  of the elements of interest in the ICP-multi-element standard solution along with two blanks consisting of the DI water used in the tests acidified with the same amount of nitric acid.

Sulfide analysis was carried out by an UV-Vis spectrophotometer (Macherey-Nagel, Nanocolor UV/Vis II). The specific Macherey-Nagel test kit for sulfide (NANOCOLOR test tube 985073), based on the methylene blue method, was used to measure all the samples. The difference between total sulphur and sulfide was used to determine the sulfate content in the model solutions, assuming that the formation of sulphite was negligible, as well as thiosulfate, which is not stable in SCW [28].

Total carbon (TC), total organic carbon (TOC), and total inorganic carbon (TIC) contents of WBL samples were analysed using a TOC analyser (Dimatoc, Dimatec Analysentechnik, Germany), and TIC was used to calculate the  $\text{CO}_3^{2-}$  concentration. The samples diluted to the calibrated concentration range and maintained under stirring were injected into a quartz glass reactor where they were burnt at 850  $^\circ\text{C}$  under a constant oxygen carrier gas flow (200  $\text{mL}\cdot\text{min}^{-1}$ ).  $\text{CO}_2$  was detected with a non-dispersive infrared (NDIR) detector for determining the TC. For measuring the TIC, the samples were injected into a 10 wt% solution of  $\text{H}_3\text{PO}_4$ , and the evolving  $\text{CO}_2$  was stripped with the oxygen carrier gas flow and transported to the NDIR detector. Then, the TOC was obtained by subtracting the TIC from the TC. The analysis was repeated around seven times for each sample (standard deviation evaluation).

Hereafter, any reported errors pertain to the standard deviation sample analysis. Uncertainty propagation for confidence interval calculations was conducted assuming no correlation between variables. Error bars denote confidence intervals derived from the estimated standard error of the mean.

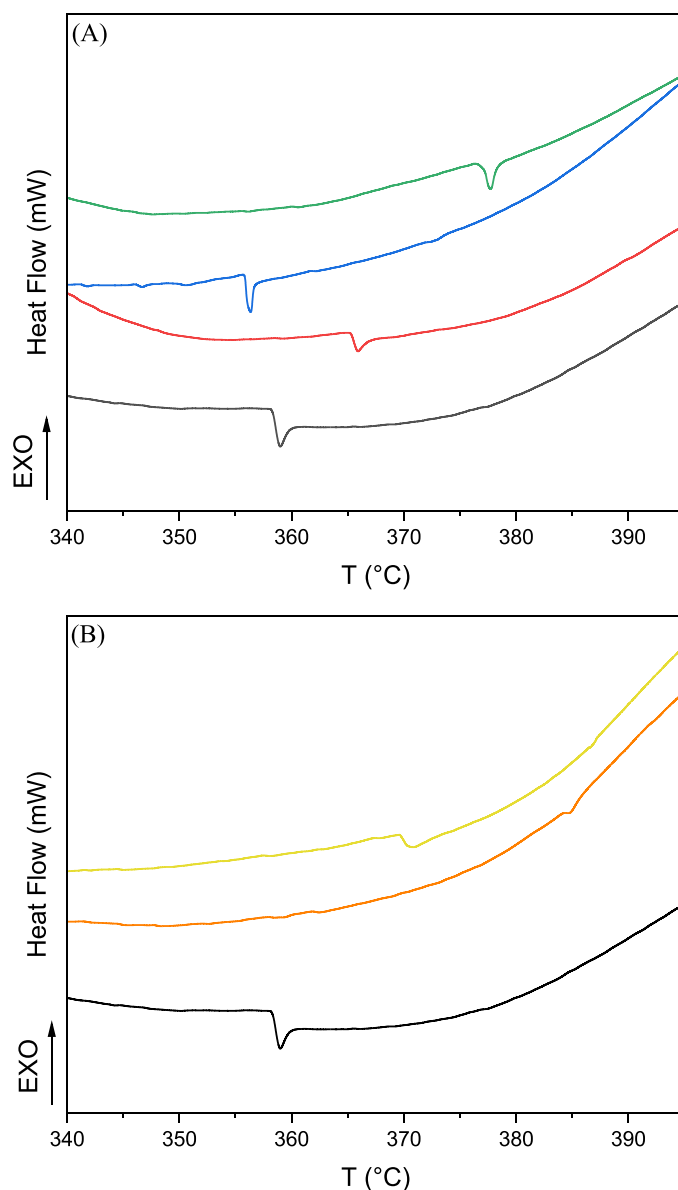


**Fig. 2.** HP-DSC traces of model salt solutions with varying concentrations of NaOH and NaHS; (A): (–) Model salt solution based on WBL characterisation (Experiment A); (–) doubling NaOH (Experiment B); (–) doubling NaSH (Experiment D); (–) doubling NaOH and NaHS (Experiment E); (B): (–) 25% of carbonate (Experiment F), (–) 50% of carbonate reduction (Experiment G).

#### 2.5. Thermodynamic modelling of acetate dissolution

Due to the scarcity of information on the solubility of sodium and potassium acetates in pure water at elevated temperatures and

pressures, the solubilities of the ternary mixture of water and the pure organic salts and their mixture were estimated using the GEMS software [42]. The standard thermodynamic properties were obtained from literature, and the PSI/Nagra and sprct98 databases were considered in the calculations. The activity coefficients of aqueous species were calculated using the Debye-Hückel equation and a more detailed description of the software calculations can be found elsewhere [43]. The solid and aqueous species considered in the estimation are listed in Table 5. The concentration of both organic salts followed the amount added in the continuous tests (Table 4).

### 3. Results and discussion

#### 3.1. Studying model salt solutions by HP-DSC

##### 3.1.1. Incoloy crucibles

The phase behaviour of individual salts under SCW conditions predominantly present in WBL are readily available in literature. However, complexity arises when studying mixtures of two or more salts, which only sometimes follow a trend. Mixtures consisting of only Type 2 salts have occasionally shown to exhibit Type 1 behaviour, and *vice versa* for mixtures of Type 1 salts [33,36,44]. This is further exacerbated by the absence of a reliable model to predict the behaviour of complex salt mixtures and at various concentrations. A general understanding is that adding more Type 1 salts will induce Type 1 behaviour. While this may often be the case, it is not guaranteed, leading to a trial and error approach. Isochoric HP-DSC is an ideal method for accurately studying the phase behaviour of complex salt solutions based on WBL composition, allowing an easy differentiation for Type 1 and Type 2 salts. Good examples of HP-DSC curves for Type 1 and Type 2 salts can be found in Fig. 5 (absence of observable heat flow resulting from phase transition, or endothermic step assigned to a liquid-liquid immiscibility) and Fig. 2A (endothermic peak corresponding to precipitation), respectively.

The phase equilibria of the model salt solutions were initially studied using Incoloy crucibles provided by the manufacturer (SETERAM, France). Whilst high-Ni steels, such as Incoloy, have improved corrosion resistance in alkaline and oxidative SCW conditions [45], the resistance of these alloys in alkaline and reducing conditions are less well known. The presence of NaHS, even in small quantities, has shown to lead to noticeable corrosion of Inconel [12,46,47], which has previously led the HP-DSC crucibles to leak. Also, carbonates and hydroxides are known to inhibit and/or passivate nickel-base alloys corrosion (*e.g. Hastelloy*) in oxidative/neutral hydrothermal and supercritical water [45]. However, carbonates mixed with organics (reducing conditions) lead to fast corrosion by carbonate on Inconel 625 [48], but also to a lower extent by hydroxide [49].

As previously reported by our group [12], to avoid the corrosion of the sealed Incoloy crucibles, the concentration of NaHS was limited to 1 wt% with a temperature ramp of 1 K·min<sup>-1</sup>, as opposed to 0.1 K·min<sup>-1</sup>, to minimise exposure of the crucibles to high temperatures. Despite these efforts, the Incoloy crucibles leaked more often than not, hindering the generation of a full dataset. The leaks typically occurred at SCW conditions, which was evident from a large endothermic transition (Figure S1). Dilution of the model salt solutions by several factors to reduce corrosion had little impact, with the majority of mixtures leaking and visibly corroding the crucibles, preventing a full systematic study. Note that the crucible started to leak systematically after reaching supercritical conditions, which could occur after only a few minutes (see Figure S1 and Figure S2, representative of the several aborted analyses). An alternative approach, which was previously used by our group [12], was to replace the problematic NaHS with additional NaOH in order to mitigate the corrosion of the nickel. Both NaOH and NaHS exhibit similar DSC traces and are both Type 1 salts. This, however, had little impact on the corrosion issues, suggesting NaHS was not entirely responsible. Due to the harsh conditions required for supercritical water, limited commercial options were available for alternative crucibles that

met the specifications (500 °C, 500 bar).

##### 3.1.2. Titanium crucibles

To overcome the corrosion difficulties posed by the strong alkali nature of the model salt solutions and the SCW conditions, a decision was taken to construct crucibles of a more suitable material in house. Titanium grade 5 (Ti-6AL-4 V) was selected due to its known chemical resistance and good mechanical properties [50], and manufactured based on the dimensions of the Incoloy crucibles. The new crucibles were pre-treated in a 5 M NaOH bath for 24 h at room temperature to dissolve surface aluminium, and heat treated at 600 °C for 1 h to strengthen the alloy [51]. The titanium crucibles were pressure tested prior to being analysed in the HP-DSC, as to avoid damage of the calorimeter. The crucibles were initially tested with water (300 kg·m<sup>-3</sup> internal density) in a furnace heated to 430 °C, followed by testing with model salt solution. The mass of the crucibles before and after heating indicated that there were no leakages. There were no visible signs of corrosion to the crucibles either. A HP-DSC analysis of pure water in the titanium crucible was performed (Figure S3), with a critical temperature of 373.83 °C, compared to 373.96 °C from the NIST reference database [39], with the difference being caused by an overcooling phenomenon [38], as for the Incoloy crucibles.

The phase behaviour of the model salt solutions was determined using the titanium crucibles. Based on the results obtained from the characterisation, experiment A in Table 2 represents the composition of the WBL and serves as a reference point for optimisation to induce Type 1 behaviour. Initial experiments were performed without the presence of organics, in order to see the effect purely based on the salt composition. Experiments B-D are adjustments to the compositions of A with increasing concentrations of NaOH and NaHS, individually and collectively. NaHS has previously shown to exhibit Type 1 behaviour [12], and increasing the overall concentration, along with NaOH, could potentially induce Type 1 salt separation under SCW conditions. An advantage of the titanium over the Incoloy crucibles was that temperature scanning rates could be performed at 0.1 °C min<sup>-1</sup>, to allow for greater resolution of the DSC trace.

The heat flow curves of the model salt solutions do not appear to show a gradual endothermic transition, as is typically seen for supercritical water (Figure S3). The endothermic curve results from increasing enthalpy with the increasing temperature, followed by a pronounced exothermic transition due to the supercritical transition. This is due to the disappearance of the gas-liquid interface forming a single homogeneous fluid (G-L → F). The heat flow curve of experiment A has an endothermic peak at 358.8 °C indicative of a Type 2 salt separation (Fig. 2), resulting from precipitation. A gradual exothermic transition is seen after the precipitation, with no clear supercritical transition. Such behaviour has previously been observed [12]. An increase in the concentration of NaOH to 3.49 wt% (experiment B) sees similar behaviour to that of experiment A, with the precipitation transition shifted to 366.0 °C. The higher temperature suggests greater solubility with the addition of NaOH, in line with a lower heat flow, i.e. less salt precipitated. Increasing the concentration of NaHS (experiment C), however, sees the crystallisation occur at 356.4 °C, lower than that of the reference point experiment A. The oxidation of the NaHS is unlikely because of the purging of the crucibles with argon prior to sealing. Increasing the concentrations of NaOH and NaHS to 3.49 and 1.20 wt%, respectively, results in a significant increase in the precipitation temperature to 377.8 °C (experiment D), above the critical point of water. As the supercritical transition is not clearly visible from the heat flow curve, it is difficult to determine where the transition occurs. A possibility of reaction occurring between the titanium crucible and residual aluminium present due to the alkaline conditions could play a role in the phase behaviour. However, there is no clear evidence of this, and the absence of a clear transition observed with an alkaline salt mixture in an Incoloy crucible [12] indicates that the cause is elsewhere.

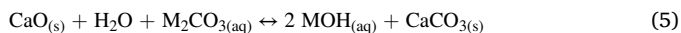
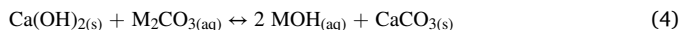
Increasing the concentrations of NaOH and NaHS (Fig. 2A) appears

to affect the precipitation temperatures of the model salt solutions, however it shows little impact on inducing Type 1 phase behaviour. All model salt solutions tested (experiments A-D) exhibit heat flow curves typical of Type 2 salts. This is true also for the model salt solutions containing organics (experiments J-M), which follow similar trends in crystallisation as for experiments A-D (Figure S4). The only significant difference is the shifting of the endothermic precipitation peak to higher temperature in the presence of organics. The approach of increasing the concentrations of Type 1 salts present in WBL appears not to be suited for inducing Type 1 or preventing Type 2 phase behaviour, but might still have benefits in a continuous separation process. An alternative approach is required. It could be argued that the presence of organics may allow for lower salt separation due to an increase in the overall density of the fluid. This is in phase with the HP-DSC curves.

Initial HP-DSC runs of the model salt solutions containing 25% (Exp. E) and 50% (Exp. F) of the sodium carbonate (other salts kept constant) of the reference model salt solution (Exp. A) appear to exhibit Type 1 behaviour (Fig. 2B). The absence of a supercritical water phase transition has previously been linked to Type 1 phase separation [12]. An endothermic step is visible for Exp. F, which illustrates the transition from L-G to an L + F phases. Further reduction in carbonate content, Exp. G (Fig. 2B), sees this transition increase from 372 °C to 378 °C, suggesting a more suitable approach is to remove Type 2 salts in order to induce an overall Type 1 behaviour.

### 3.1.3. Causticisation of model salt solutions

An alternative strategy to induce Type 1 salt behaviour, which to our knowledge has not been explored in literature, is to selectively remove Type 2 salts present in WBL. The predominant Type 2 salt anions present in WBL are sulfates and carbonates, which are present in relatively high concentrations. The substitution of these anions have been reported extensively, with uses of NaBO<sub>2</sub> [52,53], Na<sub>2</sub>SiO<sub>3</sub> [54], TiO<sub>2</sub> [55–57] and Ba(OH)<sub>2</sub> [58] having shown appreciable ion exchange efficiencies. However, suitability of these methods in the Kraft process could be questioned due to poor salt recovery, fouling [53], cost and compatibility with sulphur containing compounds [59]. The proposed strategy herein is to remove carbonate present in WBL by CaO in a two-step reaction (Eqs. 3 and 4):



This causticisation process is already implemented in the Kraft process for removing metal carbonates and recycling the cooking materials, converting green liquor to white liquor [60]. The CaO can then be regenerated from CaCO<sub>3</sub> in a lime kiln at 850–900 °C [61]. The pre-existing process allows for easier inclusion of a causticisation step at an earlier stage in the Kraft process and minimises changes to the infrastructure. Moreover, the removal of CO<sub>3</sub><sup>2-</sup> is more straightforward than the removal of SO<sub>4</sub><sup>2-</sup>, and forms additional Type 1 metal hydroxide, MOH, possibly further enhancing efficient salt separation.

The causticization efficiency of CaO, i.e. the carbonate conversion in reaction (5), was found to be 89% and 87% for the neat model salt solution and organic-containing model salt solution, respectively, suggesting it to be a viable method, not significantly affected by the presence of acetate. The fact that a full causticization could not be reached might be linked to an incomplete filtration, with very small calcium carbonate particles remaining in suspension. With real WBL, a removal of inorganic carbon of 23% was found which is much lower than from the test with model solution. During the test, an increase of the viscosity was observed and filtration was found to be immensely slower. These two observations indicate the formation of many small particles that are challenging to separate, which is to the best of our knowledge the main cause of this low yield. Causticization of real black

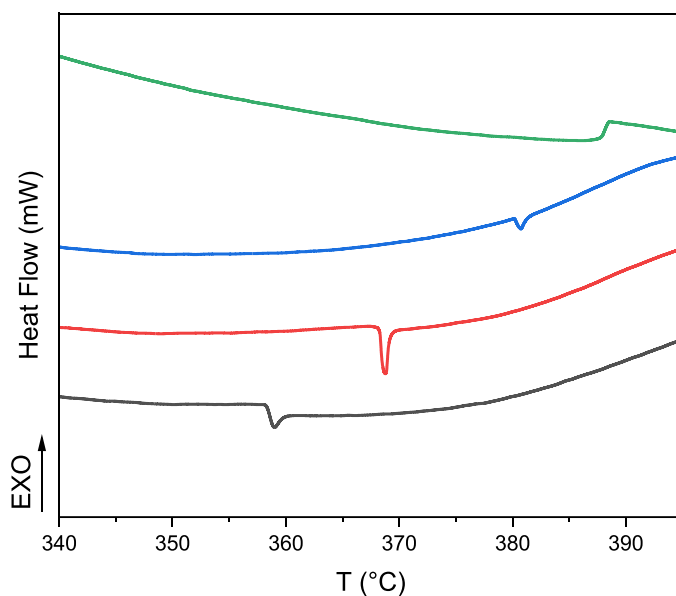


Fig. 3. HP-DSC traces of model salt solutions with simulated CO<sub>3</sub><sup>2-</sup> extraction (–), model salt solution based on WBL characterisation (Experiment A); (–) Removal of 25% of CO<sub>3</sub><sup>2-</sup> (Experiment G); (–) Removal of 50% of CO<sub>3</sub><sup>2-</sup> (Experiment H); (–) Removal of 75% of CO<sub>3</sub><sup>2-</sup> (Experiment I).

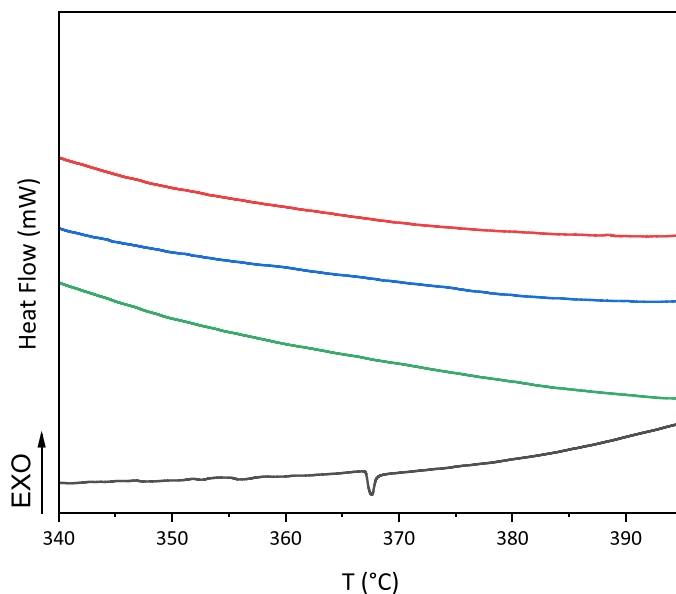


Fig. 4. HP-DSC traces of model salt solutions containing organics with simulated CO<sub>3</sub><sup>2-</sup> extraction (–), model salt solution based on WBL characterisation with the addition of acetates; (–) Removal of 25% of carbonate (Experiment N); (–) Removal of 50% of carbonate (Experiment O); (–) Removal of 75% of carbonate (Experiment P).

liquor deserves proper optimisation, with a focus on nucleation, favouring calcium carbonate particle growth, and/or using flocculation agents, an optimisation that is beyond the scope of this paper. HP-DSC analysis simulating CO<sub>3</sub><sup>2-</sup> extraction efficiencies (25%, 50%, and 75%) indicates that removal of 75% of CO<sub>3</sub><sup>2-</sup> results in a heat flow curve resembling that of water (Exp. I), however much less pronounced (see Figure S5), and could be a liquid to fluid (L → F) transition around 387 °C (Fig. 3). The absence of a strong endothermic transition indicates a liquid-vapour transition to liquid-supercritical fluid phases, L-V → L + F, with the liquid being salt-rich. As the CO<sub>3</sub><sup>2-</sup> is reduced (Exp. A to I) in the model salt solutions, the endothermic crystallisation transition shifts to

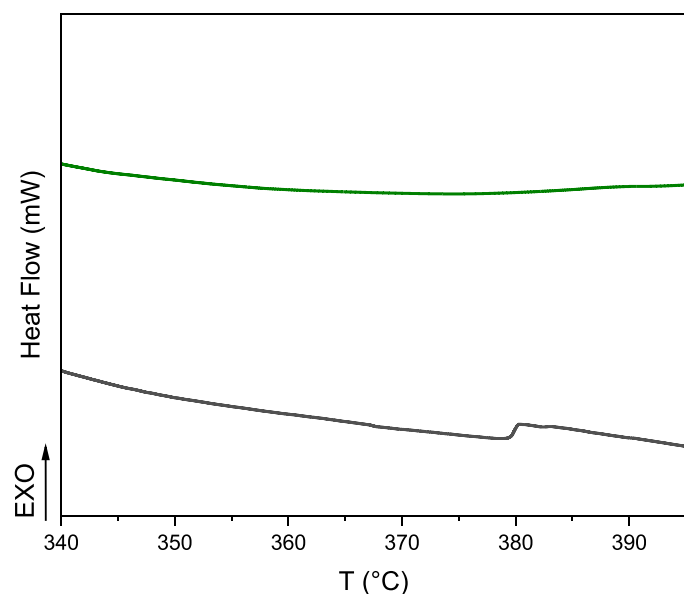


Fig. 5. HP-DSC traces of (–) organic-free model salt solution treated with CaO; and (–) organic model salt solution treated with CaO. The reference experiment with full carbonate concentration is experiment J.

higher temperatures. This is likely due to the increasing concentration of MOH present as seen in (Fig. 2). The removal of 50% of initial carbonate (Exp. H) sees the endothermic transition significantly reduce in heat flow, with further reduction seen with 75% removal (Exp. I), in phase with a decrease of salt precipitation at the corresponding conditions.

The impact of removing  $\text{CO}_3^{2-}$  from the model salt solutions containing organics is significantly higher, with the simulated 25% extraction (Exp. N) showing no noticeable phase transitions (Fig. 4). Similar results have been observed previously with the replacement of sodium with potassium [12]. This shows that the formation of the salt-depleted supercritical fluid phase is more gradual than for model salt solutions containing no organics or higher concentrations of  $\text{CO}_3^{2-}$ . The presence of organics in the form of metal carboxylates promotes the salt separation into a salt-rich liquid phase (Type 1) and a salt-depleted supercritical fluid phase. Further increasing  $\text{CO}_3^{2-}$  extraction efficiency, and consequently the MOH, sees little change in the heat flow curves (Exps. O and P). This further suggests Type 1 behaviour of the salt solutions.

The model salt solutions treated with CaO exhibit similar heat flow curves to those of the simulated extraction samples in HP-DSC analyses, both with and without organics (Fig. 5). The organic-free model salt solution has a visible supercritical transition at 380 °C (exp. A), compared to 387 °C of the simulated extraction. There is no clear explanation for the difference in transition other than the presence of additional MOH. For the organic containing model salt solution, no noticeable transition is visible, as is seen for the simulated extraction.

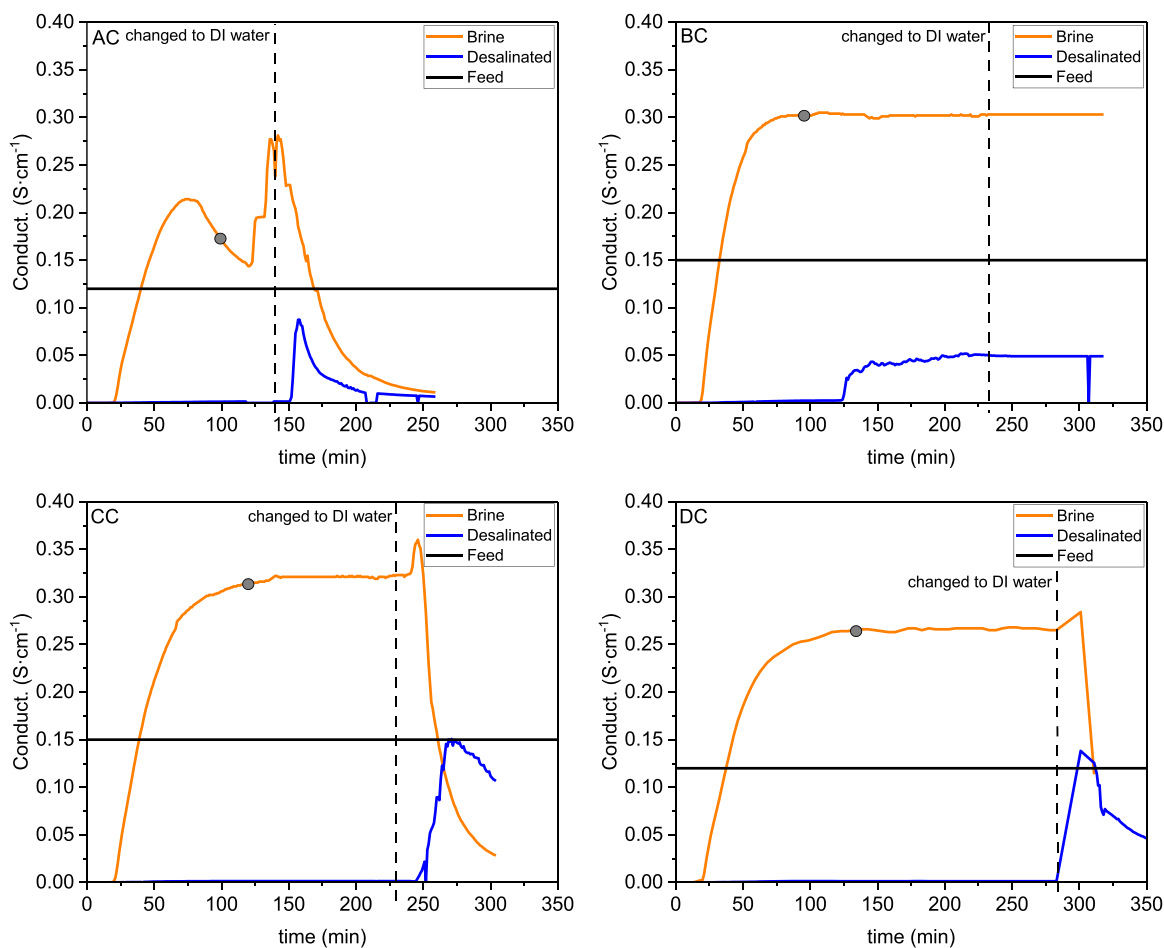


Fig. 6. Evolution of the conductivity of the brine and desalinated stream effluents for experiments with model salt solutions free of organics. Grey circles indicate the time of effluent sampling. The vertical dashed line indicates the change from feeding salts to DI water. AC, BC, CC, DC refer to the experimental conditions in Table 4.

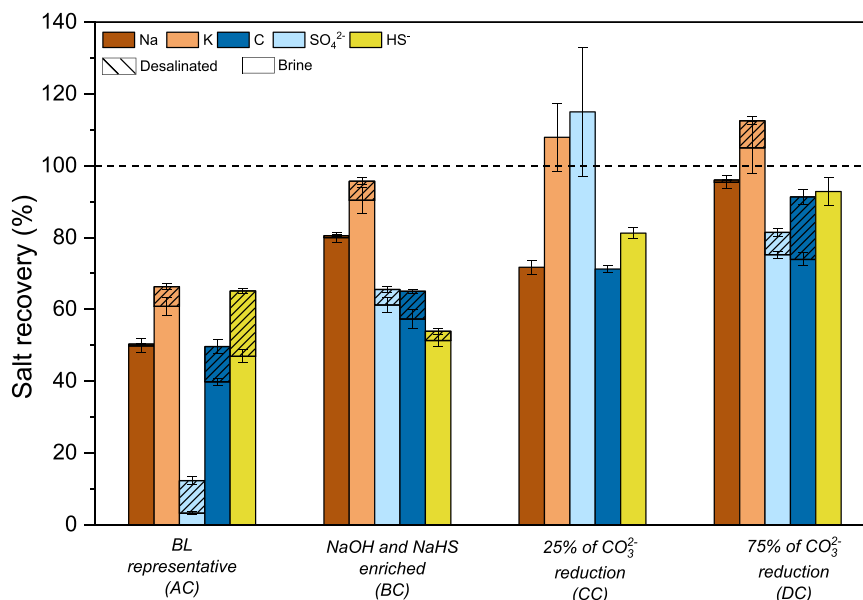


Fig. 7. Salt recovery efficiency for model salt solutions free of organics.

### 3.2. Continuous salt separation efficiency

#### 3.2.1. Model salt solutions free of organics

Fig. 6 presents the evolution of the conductivities for the brine and desalinated streams for experiments conducted on the continuous salt separation test rig without adding organics. Table 4 lists the conditions used for the experiments. Experiment AC shows the conductivity of the desalinated stream to remain constant and lower than  $0.01 \text{ S cm}^{-1}$  throughout the experiment after feeding the model salt solution. The feed conductivity is  $0.12 \text{ S cm}^{-1}$ , indicating an efficient separation of the salts from the main stream, as the fluid passes through the supercritical region. The brine conductivity starts to increase 20 min after changing the feed to the model salt solution and achieves a maximum value of  $0.21 \text{ S cm}^{-1}$  after 75 min. This indicates that the salts can be, at least partially, extracted continuously in the brine, separating them from the desalinated stream. It is worth noting that the time delay until the brine conductivity starts to change is normal and represents the time needed for the fluids to reach the conductivity sensors.

However, the brine conductivity starts fluctuating 10 min after reaching the maximum value. At the same time, the pressure (not shown) increases suddenly, suggesting that a plug is built up inside the separation vessel. The decrease in brine mass flow rate also indicates salt accumulation, probably because of salt crystals plugging the filter upstream of the mass flow controller (see Fig. 1). As the filter is at near ambient temperature, the rate of salt redissolution might be slow due to the higher concentration of Type 2 salts in relation to Type 1 salts. Previous studies have pointed out that salts might be continuously recovered from mixtures containing Type 2 salts as long as these mixtures contain a sufficiently high concentration of Type 1 salts, the latter likely preventing the deposition of precipitates on the walls [12,32,44]. The feed was changed to DI water after 140 min, and the conductivities of both outlet streams (brine and desalinated) rapidly increased, which corroborates the assumption of an important accumulation of salts in the vessel during the experiment. Some of the Type 2 salts probably precipitate and deposit on the hot surfaces of the separation vessel, leading to the blockage of the vessel.

Fig. 7 presents the mass balance results (see also Table S1). The quantity of sodium, potassium, sulfate, carbonate, and sulfide recovered in experiment AC was  $50 \pm 2$ ,  $66 \pm 3$ ,  $12 \pm 2$ ,  $50 \pm 3$ , and  $65 \pm 3\%$ , respectively. The low salt recovery indicates salt accumulation inside the vessel, which corroborates the behaviour found in experiment AC.

The results in Fig. 2A indicate an impact of the enrichment of the reference salt mixture with NaHS and/or NaOH on the precipitation temperature, while precipitation is still favoured. In order to evaluate the real impact of the enrichment of both NaHS and NaOH on the phase behaviour of the salt mixture, the experiment BC was conducted on our continuous setup. As shown in Fig. 6, the brine conductivity starts to increase after 20 min and achieves a twofold value of feed conductivity after about 55 min, suggesting a salt enrichment in the brine stream. As the feed conductivity is  $0.11 \text{ S cm}^{-1}$ , the conductivity values for desalinated and brine streams indicate the salt separation from the mainstream as the fluid passes throughout the supercritical region. The conductivity of the desalinated stream starts to increase slightly 23 min after changing the feed to the model salt solution. The conductivity keeps slowly increasing until 125 min when a sudden increase to  $0.05 \text{ S cm}^{-1}$  between 125 and 225 min happens. A logical explanation of this behaviour is that the brine flow is not high enough to prevent salts (liquid, dissolved or precipitated) from accumulating in the separation vessel and then overflowing by the top outlet of the vessel to the desalinated stream outlet. The presence of carbonate anions might also present drawbacks for the salt separation efficiency, since there is no overflowing in experiments with reduced carbonate concentration (CC and DC) and it has a low solubility in SCW. Yang et al. [20] listed the solubility of anions with the same counter cation as  $\text{NO}_3^- > \text{Cl}^- > \text{H}_2\text{PO}_4^- > \text{HPO}_4^{2-} > \text{PO}_4^{3-} > \text{SO}_4^{2-} > \text{CO}_3^{2-}$ . The difficulty of carbonate in forming hydrogen bonds [20] and the stability of carbonic acid at high pressure and high temperature [62] results in poor dissociation, directly affecting the anion solubility in water and enabling the salts to overflow by the top. According to the mass balance results (Fig. 7, experiment BC), the salt recovery is  $80 \pm 2$ ,  $96 \pm 5$ ,  $66 \pm 3$ ,  $64 \pm 4$ ,  $46 \pm 3$  and  $54 \pm 3\%$  for sodium, potassium, sulfate, carbonate, and sulfide, respectively. The strategy of increasing salt Type 1 concentration in the neat solutions presents a positive impact. However, in this case the Type 1 character is insufficient to prevent salt accumulation inside the vessel, as the mass balance is not closed. The results indicate an accumulation of salts inside the separator, which may be caused by a too low brine flow rate or a poor redissolution of Type 2 salts by the Type 1 salts in the neat solution. The hypothesis that the brine flow rate is not high enough might indicate the presence of solid salt particles favouring accumulation in the vessel. However, the absence of a decrease in brine conductivity or a sign of salt plugging during the test is a positive outcome. It indicates that the optimisation of a continuous salt separation process can employ this

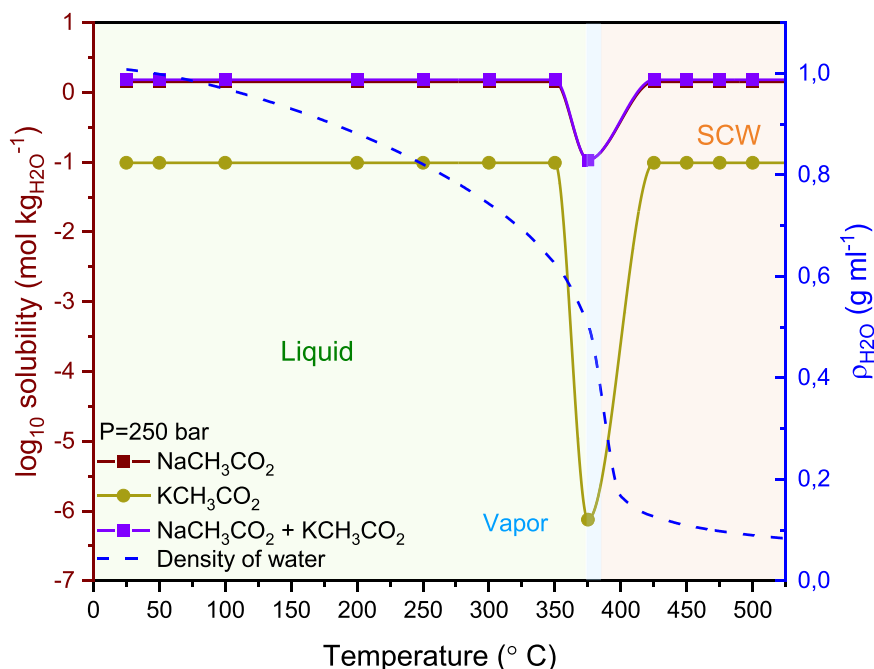


Fig. 8. Solubility estimation of  $\text{NaCH}_3\text{CO}_2$  ( $1.4 \text{ mol}\cdot\text{kg}^{-1}$ ),  $\text{KCH}_3\text{CO}_2$  ( $0.098 \text{ mol}\cdot\text{kg}^{-1}$ ) and  $\text{NaCH}_3\text{CO}_2 + \text{KCH}_3\text{CO}_2$  in pure water ( $1.4 \text{ mol}\cdot\text{L}^{-1}$ ) as a function of temperature at 250 bar.

strategy. The study performed by Schubert et al. [44] showed that for electrolyte solutions containing Type 1 salts ( $\text{KNO}_3$  and  $\text{NaNO}_3$ ), decreasing the brine flow rate increased the salt concentration in the brine up to more than 10 times the feed concentration. In this case, the authors worked with binary mixtures and did not take into account the influence of brine flow rate of the salt separation for multicomponent mixtures containing both Type 1 and Type 2 salts.

The predominant Type 2 anions in WBL composition are sulfates and carbonates, and as aforementioned, carbonate extraction presents the potential to be a suitable method to induce global Type 1 behaviour. Experiment DC (Fig. 6) shows the evolution of the effluent conductivities in which a model salt solution simulates an extraction of 75% of carbonate (replaced by sodium hydroxide, see Eqs. 2 and 3). The desalinated stream conductivity increases 5 min after feeding the model solution into the separator and remains lower than  $0.01 \text{ S}\cdot\text{cm}^{-1}$  throughout the experiment. At the top of the vessel, the conductivity of the outlet stream starts to increase after 18 min and achieves a maximum value of  $0.32 \text{ S}\cdot\text{cm}^{-1}$ , which indicates salt enrichment in the brine stream. The feed conductivity is  $0.15 \text{ S}\cdot\text{cm}^{-1}$ , so the salts effectively separate from the inlet stream as the fluid passes through the supercritical region. It is worth noting that there is no plug formation during the experiment, allowing to conduct the continuous hydrothermal process for approximately 4 hours. These results align with the HP-DSC data (Fig. 2B), which shows the absence of a precipitation peak in the temperature range of the experiment.

As presented in Fig. 6, the carbonate reduction of 25% (experiment CC) positively affects the continuous hydrothermal process resulting in plug-free operation throughout the experiment. This contradicts the HP-DSC results exhibiting a small precipitation peak at  $382^\circ\text{C}$ . By comparing the experiments DC and CC, one can observe a lower value of the brine conductivity in experiment DC after reaching the steady-state value. This is likely due to the formation of a phase equilibrium between a fluid and a solid phase containing a high amount of carbonates (Type 2 salt), which might slow down its redissolution by the brine.

The mass balance (Fig. 7) presents interesting results about salt recovery efficiency for both experiments CC and DC. The quantity of sodium, potassium, sulfate, carbonate, and sulfide recovered in experiment CC is  $72 \pm 2$ ,  $108 \pm 10$ ,  $115 \pm 18$ ,  $71 \pm 3$  and  $81 \pm 2\%$ ,

respectively. On the other hand, experiment DC presents a salt recovery of  $96 \pm 2$ ,  $112 \pm 14$ ,  $81 \pm 2$ ,  $91 \pm 2$  and  $93 \pm 4\%$  for sodium, potassium, sulfate, carbonate, and sulfide, respectively. The high salt recoveries in experiment DC confirm the carbonate reduction of 75% as a good strategy for continuous salt separation. For experiment CC, although presenting a promising apparent phase behaviour, the mass balances for sodium, carbon and sulfide indicate accumulation in the separation vessel.

### 3.2.2. Model salt solutions containing organics

The strategies to prevent salt precipitation evaluated for the inorganic model salt solutions free of organics have proven efficient for continuous separation in the HTL process. However, as WBL contains a high concentration of organic compounds, investigating the influence of organic compounds and, most importantly, organic salts in the salt separation efficiency is primordial. To evaluate the impact of the numerous carboxylate salts in weak black liquor on the salt separation efficiency, sodium and potassium acetate were added to the model salt solutions, chosen due to their stability in supercritical water.

The addition of organics in the WBL model salt solution (experiment EC) mainly influences the desalinated stream (Fig. 8), achieving higher conductivity values than in experiment AC. It could be inferred that the presence of organics, increasing the fluid density [37], might impact the salt precipitation since the (pseudo)-critical temperature shifts towards higher temperatures [37]. The results from HP-DSC also point to this behaviour, as the precipitation peak shifts from  $358.8$  to  $368^\circ\text{C}$  in the presence of organics. However, the small shift in the precipitation peak is not enough to change the Type 2 behaviour throughout the experiment, as the precipitation temperature remains lower than the critical temperature of the salt solution. As observed in experiment AC and already expected from HP-DSC results, experiment EC presents signs of plug formation, since the pressure fluctuates in the range of 200–320 bar throughout the test (Figure S7). Although the brine stream conductivity reaches values above the feed conductivity and the desalinated stream conductivity remains lower than  $0.01 \text{ S}\cdot\text{cm}^{-1}$  (indicative of salt separation), it does not reach a steady-state. Both effluent conductivities start to fluctuate after 75 min of feeding the model salts, and the feed was changed to DI water.

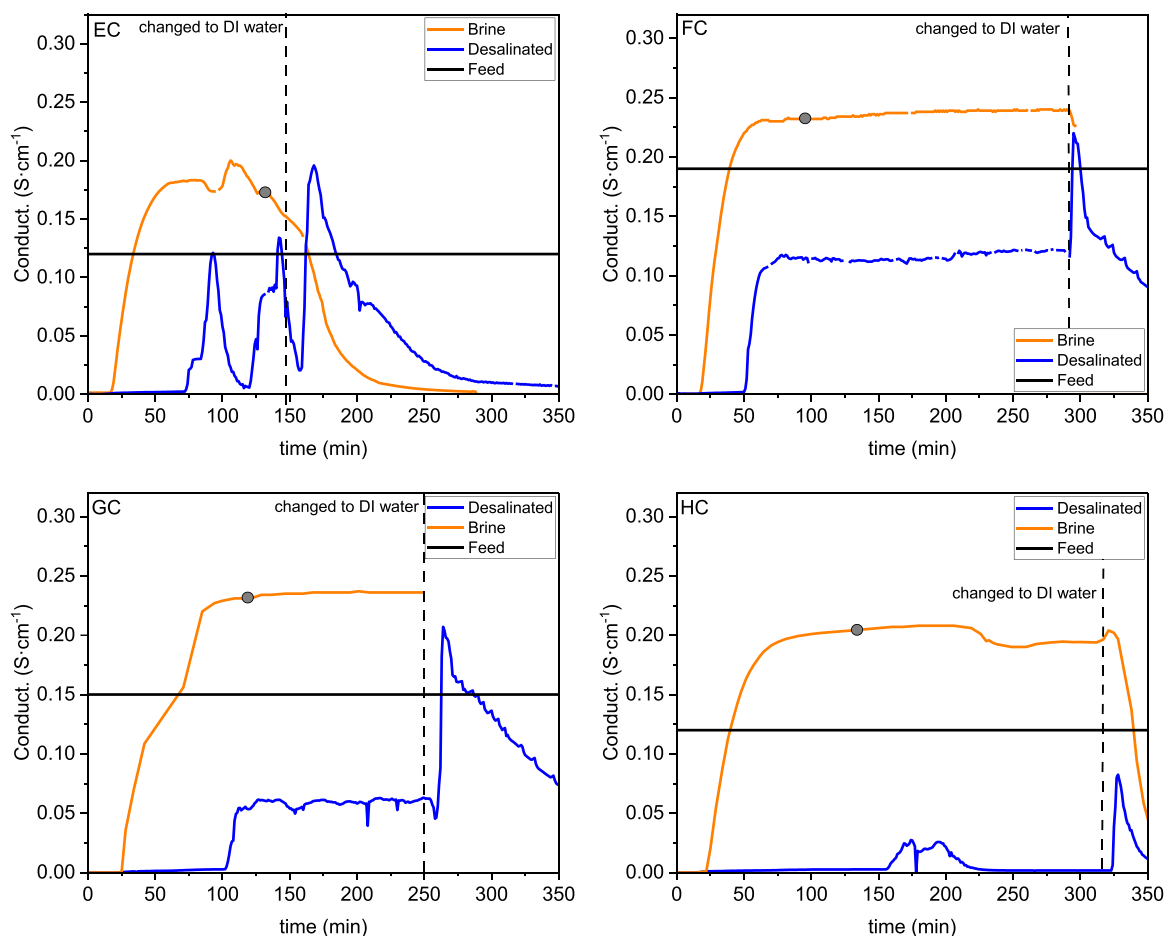


**Fig. 9.** Evolution of the conductivity of the brine and desalinated stream effluents for experiments with model salt solutions and organics. Grey circles indicate the time of effluent sampling. The vertical dashed line indicates the change from feeding salts to DI water. EC, FC, GC, HC refer to the experimental conditions in Table 4.

For experiment FC (Fig. 9), which corresponds to experiment BC with the addition of acetates, the evolution of effluent conductivities follows the same trend as for the experiment with no organic addition, except for the higher desalinated stream conductivity with organics. The presence of organics results in a high amount of salts leaving the salt separator by the top (desalinated stream), which happens much earlier than with the experiment without organics. The presence of organics seems to exacerbate the suspected overflowing of the separation vessel, which is indeed expected to fill faster in the presence of additional organic salts. Since the anion of organic salts has a low polarity, they may be well soluble in SCW and flow out at the top of the reactor. To support this hypothesis, solubility calculations of sodium and potassium acetates were done for a range of conditions similar to the salt separation experiments. At the experimental conditions at the top of the separator (250 bar, 420 °C), sodium and potassium acetates are soluble in supercritical water, which supports the aforementioned hypothesis. (Fig. 8).

Although experiment FC does not present operational issues, which means no plug is formed throughout the experiment and a steady-state is established for at least 4 hours, the overall salt recovery from the brine is low compared to the previous experiments. As presented in Fig. 10, the percentage of sodium, potassium, sulfate, total carbon, total organic carbon, and sulfide extracted are  $88 \pm 3$ ,  $91 \pm 2$ ,  $59 \pm 2$ ,  $84 \pm 2$ ,  $80 \pm 3$ , and  $97 \pm 3\%$ , respectively. It is worth noting that the high amount of sulfate and sulfide leaving the desalinated stream also indicates an unsuitable separation condition. These compounds are not desirable to be present at the top since they may poison the catalyst during the catalytic conversion of the desalinated stream.

The low salt separation efficiency in the brine stream can be related

to the presence of carbonates and organics, which negatively affect the salt separation [37]. Decarboxylation of organics in such conditions is a plausible explanation for understanding the salt deposition inside the vessel. Since part of the organics could be converted into carbonates via decarboxylation [15], this additional carbonate increases the concentration of Type 2 salts inside the separator. As a result, the redissolution rate of the salts precipitating at the bottom due to the increase of type 2 salts in the vessel can cause an overflowing at the top.

Similar to the behaviour observed for the experiments with no addition of organics (Fig. 6, Exp. DC), experiment GC (Fig. 8) confirms the positive influence in reducing carbonate concentration by 75% even in the presence of acetates. It is worth noting that there is a delay in the increase of desalinated conductivity when compared to exp. FC, also suggesting a positive effect of carbonate reduction. The brine conductivity starts to increase just after 25 min of feeding the salt separator with the model salt solution. In comparison, the desalinated stream conductivity remains lower than  $0.01 \text{ S cm}^{-1}$  during the first 100 min of operation. After that, the desalinated stream conductivity suddenly reaches a value of  $0.05 \text{ S cm}^{-1}$ . As the brine effluent conductivity remains at the same level, this behaviour might be an indicator of overflowing due to salt accumulation inside the vessel. Adopting a higher brine flow rate could potentially counter the overflow issue, preventing the formation of salt deposits and enhancing the flushing out of the organic salts, which might be soluble in subcritical water from the bottom. The increase in the brine flow rate has a positive impact in experiment HC. According to Fig. 8, associating the reduction of 25% of carbonate concentration with the increase of brine flow rate contributes to a steady continuous process and decreases the risk of plugging due to

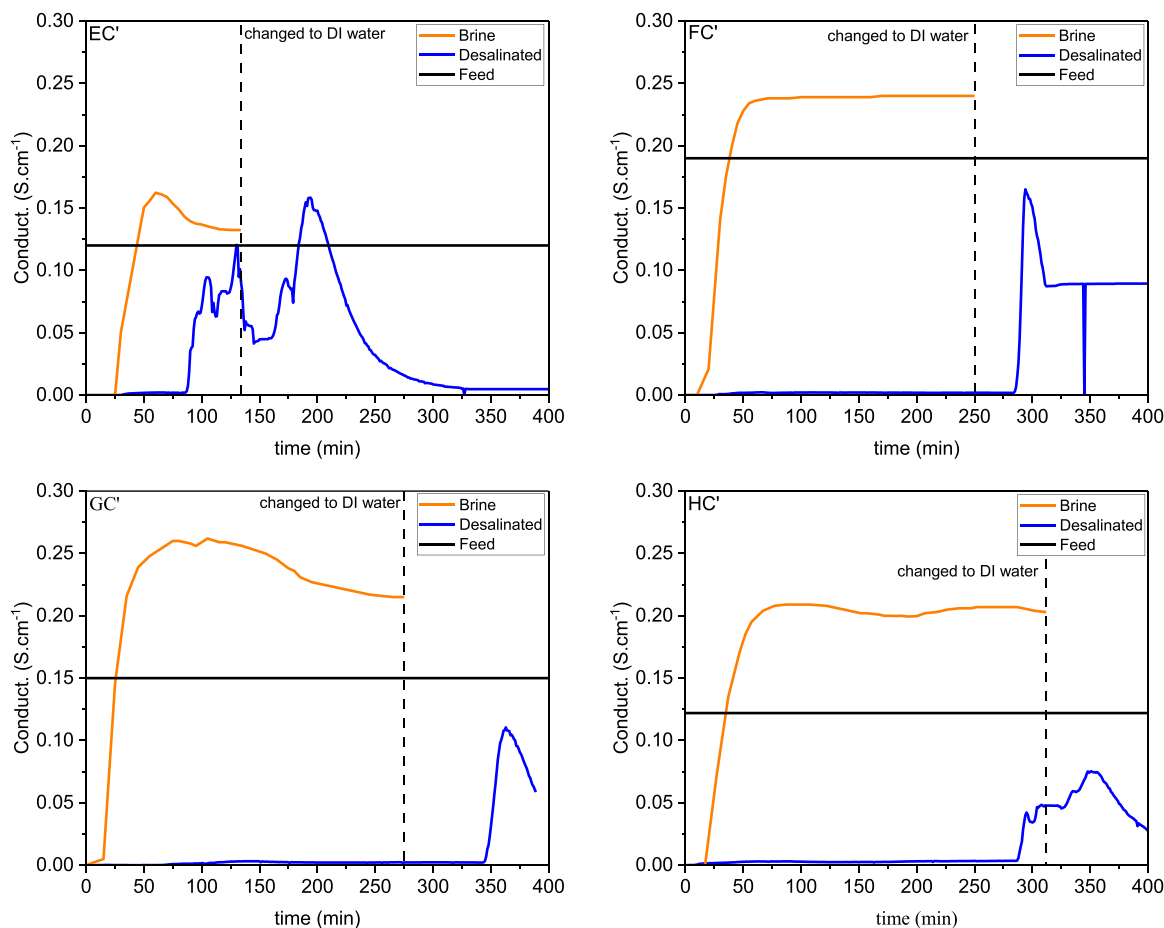


**Fig. 10.** Effect of a 40% increase of the brine flow rate on the conductivity of the brine and desalinated stream effluents for experiments with model salt solutions and organics. The vertical dashed line indicates the change from feeding salts to DI water. EC', FC', GC', HC' refer to the experimental conditions in Table 4 but with a higher brine flow rate.

salt deposits. The brine conductivity starts to increase 25 min after feeding the salt separator with the model salt solution and reaches a plateau after 100 min of operation. The conductivity of the desalinated stream exhibits a behaviour similar to that observed in exp. CC (Fig. 6), with the exception of an event occurring between 150 and 225 minutes. There are two possibilities to explain this behaviour: (1) the salt solution is not able to solubilise the precipitated salts from the top due to the Type 2 salt solution nature, and the salts starts to deposit inside the vessel resulting in overflowing; (2) a plug starts to build up somewhere in the separator. The last assumption has a small probability of happening since there is no significant change in the system pressure throughout the experiment (Figure S8). Increasing the brine mass flow rate from  $2.5 \text{ g}\cdot\text{min}^{-1}$  to  $3.2 \text{ g}\cdot\text{min}^{-1}$  after this event brings the desalinated stream conductivity back to the initial value, confirming an accumulation of salts in the vessel, most likely because the brine flow rate was too low. The results indicate that increasing the brine mass flow rate is a promising strategy to avoid salt accumulation.

The influence of the brine flow rate on the salt separation was analysed by performing experiments with brine mass flow rates 40% higher than those of the experiments EC to GC. For simplicity, the experiments are referred to as EC', FC', GC', and HC' (Fig. 9). The increase in the brine flow rate does not affect the behaviour of experiment EC', since the fluctuation in the desalinated stream conductivity and the pressure of the system present the same trend as experiment EC. On the other hand, there are no signs of overflowing in experiments FC' and GC' since desalinated stream conductivity values remain roughly constant at  $0.01 \text{ S}\cdot\text{cm}^{-1}$  throughout the experiments. It is worth noting that increasing the brine flow rate might improve the solubilisation of Type 2

salts by Type 1 salts, as a higher amount of the neat solution flows through the bottom of the vessel. The absence of any signs of plugging supports this statement. In the absence of improved solubilisation, an increase in the brine flow rate serves to flush the bottom, effectively removing Type 2 salts in solid form. However, this may potentially lead to downstream filter plugging. The behaviour of experiment HC' follows a similar trend as experiment EC, except for the delay in the increase of desalinated stream conductivity. While for the experiment EC, the desalinated stream conductivity starts to increase after 150 min of continuous operation, a similar behaviour occurs in experiment HC' after 300 min. This points out the importance of process parameter optimisation along with the application of strategies to prevent Type 2 salts behaviour.

The results from Fig. 10 show high salt recovery, except for sulfate. The recovery for sodium, potassium, total carbon, total organic carbon, and sulfide was higher than 95%, while the sulfate recovery just reached 35%. The presence of organic compounds results in the extraction of a significant quantity of salts in the desalinated stream. Since the presence of organic compounds might increase the density of the fluid [37], it is the only apparent explanation for the increase of salt concentration at the top. However, a proof of this influence is lacking, and additional experiments under different conditions are necessary to support this hypothesis. Additionally, the process removes the majority of salts from the brine stream, which can have a positive impact on the gasification of the desalinated stream.

Both strategies to induce a Type 1 salt behaviour of the model salt solutions affect salt recovery efficiency positively. As already discussed in the last section, besides providing smooth operation with no system

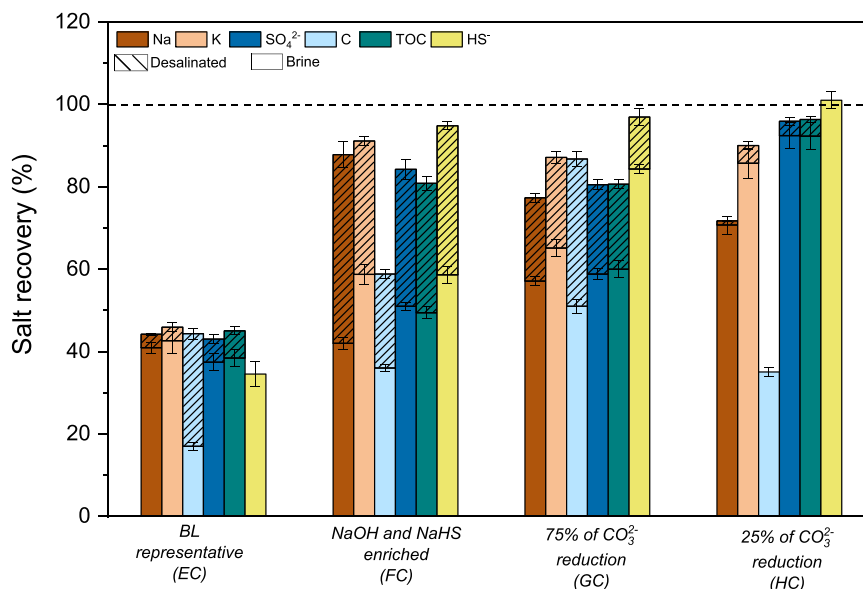


Fig. 11. Salt recovery efficiency for model salt solutions containing organics.

clogging, reducing 75% of the carbonate concentration (Exp. DC) also results in higher salt recovery efficiency. It also indicates a low level of salt accumulation in the test rig throughout the experiment since the mass balances are practically closed. The addition of organics affects the salt recovery (see Fig. 10), resulting in an increment in the salt recovery in the desalinated stream in some cases (see exp. FC and GC). A comparison between experiments GC and HC shows that besides carbonate reduction, the control of process parameters such as stream flow rates (feed, top, and bottom) are important for improving the salt separation. Except for total sulfate recovery, experiment HC clearly shows the highest salt recovery probably due to the higher brine flow rate adopted in this experiment. Comparing it with experiment GC, the 40% increase of the brine flow rate in experiment HC might facilitate the extraction of Na, K, C, TOC, and S from the bottom. Therefore, a deeper investigation of the impact of process parameters on salt separation of multi-component mixtures is granted.

#### 4. Conclusions

Developing strategies to prevent salt deposition for the process involving the conversion of wet biomass into biofuels by hydrothermal liquefaction (HTL) and hydrothermal gasification (HTG) has proven to be primordial. The phase behaviour of the salts present in the black liquor of interest, being initially unknown, has been investigated by HP-DSC using model salt solutions and presents Type 2 behaviour. Increasing the concentration of the Type 1 salts (NaOH and NaSH) extended the precipitation temperature but does not avoid salts to accumulate. Causticisation is an effective strategy, replacing Type 2 carbonate anions with hydroxide. The HP-DSC results confirm the efficiency since the Type 1 behaviour is observed after removing 75% of carbonate. In the presence of organics, some salt accumulation and overflow into the desalinated stream occurs, which can be addressed by optimising the brine flow rate. Our group's previous work [44] showed that reducing the brine flow rate increases the concentration of Type 1 salts in the brine. However, there is no observation about the concentration of Type 2 salt, which may deposit and stick on the salt separator wall causing fouling and clogging. In this study, even though the tests for multicomponent mixtures with higher amounts of Type 1 salts (Exps. BC and FC) present type 1 salt behaviour, the high concentration of Type 2 salts should still be considered. Increasing the brine flow rate prevents the salts from overflowing since a higher amount of the neat solution will flow through the bottom of the vessel, which might improve the

redissolution rate of Type 2 salts by the brine containing Type 1 salts. This study presents important advancements in mitigating salt fouling by integrating salt separation and HTL of WBL. The strategies applied are promising and provide valuable insights for scaling up the hydrothermal liquefaction of weak black liquor.

#### CRediT authorship contribution statement

**Nicholas I. Canabarro:** Writing – original draft, Methodology, Investigation, Formal analysis, Conceptualization. **Darius Yeadon:** Writing – original draft, Methodology, Investigation, Formal analysis. **Maximilian Wörner:** Writing – review & editing, Formal analysis. **Ursel Hornung:** Writing – review & editing, Formal analysis. **Frédéric Vogel:** Writing – review & editing, Visualization, Supervision. **David Baudouin:** Writing – review & editing, Validation, Supervision, Methodology, Conceptualization.

#### Declaration of Competing Interest

The authors declare that they have no known competing financial interests or personal relationships that could have appeared to influence the work reported in this paper.

#### Data availability

Data will be made available on request.

#### Acknowledgements

This research was funded by the European Union Horizon 2020 research and innovation program under grant agreement No. 884111, Black Liquor to Fuels (BL2F). The authors thank Miron George-Dan (PSI) for all the support provided during the solubility calculation with the GEMS software.

#### Appendix A. Supporting information

Supplementary data associated with this article can be found in the online version at [doi:10.1016/j.supflu.2024.106230](https://doi.org/10.1016/j.supflu.2024.106230).

## References

- [1] International Energy Agency, World Energy Outlook 2022, IEA, 2022. ([www.iea.org](http://www.iea.org)).
- [2] A.A. Peterson, F. Vogel, R.P. Lachance, M. Fröling, M.J. Antal, Jr, J.W. Tester, Thermochemical biofuel production in hydrothermal media: a review of sub- and supercritical water technologies, *Energy Environ. Sci.* 1 (2008) 32, <https://doi.org/10.1039/b810100k>.
- [3] P. Casademont, J. Sánchez-Oneto, A.P.J. Scandellai, L. Cardozo-Filho, J.R. Portela, Hydrogen production by supercritical water gasification of black liquor: use of high temperatures and short residence times in a continuous reactor, *J. Supercrit. Fluids* 159 (2020) 104772, <https://doi.org/10.1016/j.supflu.2020.104772>.
- [4] E. Miliotti, S. Dell'Orco, G. Lotti, A. Rizzo, L. Rosi, D. Chiamonti, Lignocellulosic ethanol biorefinery: valorization of lignin-rich stream through hydrothermal liquefaction, *Energies* 12 (2019) 723, <https://doi.org/10.3390/en12040723>.
- [5] C.A. Cardona Alzate, M. Ortiz-Sanchez, J.C. Solarte-Toro, Design strategy of food residues biorefineries based on multifeedstocks analysis for increasing sustainability of value chains, *Biochem. Eng. J.* 194 (2023) 108857, <https://doi.org/10.1016/j.bej.2023.108857>.
- [6] International Energy Agency (IEA), Sankey diagrams, (2023). (<https://www.iea.org/sankey/>).
- [7] A. Lawrence, P. Thollander, M. Karlsson, Drivers, barriers, and success factors for improving energy management in the pulp and paper industry, *Sustainability* 10 (2018) 1851, <https://doi.org/10.3390/su10061851>.
- [8] L. Pola, S. Collado, P. Oulego, M. Díaz, Kraft black liquor as a renewable source of value-added chemicals, *Chem. Eng. J.* 448 (2022) 137728, <https://doi.org/10.1016/j.cej.2022.137728>.
- [9] A.K. Mathew, A. Abraham, K.K. Mallapureddy, R.K. Sukumaran, Lignocellulosic Biorefinery Wastes, or Resources? *Waste Biorefinery Elsevier*, 2018, pp. 267–297, <https://doi.org/10.1016/B978-0-444-63992-9.00009-4>.
- [10] A. Mathanker, D. Pudasainee, A. Kumar, R. Gupta, Hydrothermal liquefaction of lignocellulosic biomass feedstock to produce biofuels: parametric study and products characterization, *Fuel* 271 (2020) 117534, <https://doi.org/10.1016/j.fuel.2020.117534>.
- [11] S. Maitz, M. Siebenhofer, M. Kienberger, Conversion of carbohydrates to carboxylic acids during hydrothermal and oxidative treatment of concentrated kraft black liquor, *Bioresour. Technol. Rep.* 19 (2022) 101148, <https://doi.org/10.1016/j.biteb.2022.101148>.
- [12] R. Wang, R. Deplazes, F. Vogel, D. Baudouin, Continuous extraction of black liquor salts under hydrothermal conditions, *Ind. Eng. Chem. Res.* 60 (2021) 4072–4085, <https://doi.org/10.1021/acs.iecr.0c05203>.
- [13] O. Asafu-Adjaye, B. Via, B. Sastri, S. Banerjee, Dewatering black liquor and lignin with supercritical CO<sub>2</sub>, *Fuel* 319 (2022) 123742, <https://doi.org/10.1016/j.fuel.2022.123742>.
- [14] C. De Blasio, S. De Gisi, A. Molino, M. Simonetti, M. Santarelli, M. Björklund-Sänkiah, Concerning operational aspects in supercritical water gasification of kraft black liquor, *Renew. Energy* 130 (2019) 891–901, <https://doi.org/10.1016/j.renene.2018.07.004>.
- [15] J. Lappalainen, D. Baudouin, U. Hornung, J. Schuler, K. Melin, S. Bjelić, F. Vogel, J. Konttinen, T. Joronen, Sub- and supercritical water liquefaction of kraft lignin and black liquor derived lignin, *Energies* 13 (2020) 3309, <https://doi.org/10.3390/en13133309>.
- [16] R. Morya, M. Kumar, I. Tyagi, A. Kumar Pandey, J. Park, T. Raj, R. Sirohi, V. Kumar, S.-H. Kim, Recent advances in black liquor valorization, *Bioresour. Technol.* 350 (2022) 126916, <https://doi.org/10.1016/j.biortech.2022.126916>.
- [17] M. Huet, A. Roubaud, C. Chirat, D. Lachenal, Hydrothermal treatment of black liquor for energy and phenolic platform molecules recovery in a pulp mill, *Biomass. Bioenergy* 89 (2016) 105–112, <https://doi.org/10.1016/j.biombioe.2016.03.023>.
- [18] Y. Zhao, Y. Tian, H. Zhou, Y. Tian, Hydrothermal conversion of black liquor to phenolics and hydrochar: characterization, application and comparison with lignin, *Fuel* 280 (2020) 118651, <https://doi.org/10.1016/j.fuel.2020.118651>.
- [19] P. Ranganathan, Techno-economic analysis of renewable fuels production from sewage sludge through hydrothermal liquefaction, *Sustain. Energy Technol. Assess.* 57 (2023) 103164, <https://doi.org/10.1016/j.seta.2023.103164>.
- [20] W. Yang, D. Xu, G. Jiang, Z. Jing, Y. Guo, S. Wang, B. Wang, Inorganic salts crystallization and deposition characteristics and mechanisms in supercritical water, *Desalination* 540 (2022) 116016, <https://doi.org/10.1016/j.desal.2022.116016>.
- [21] S. van Wyk, A.G.J. van der Ham, S.R.A. Kersten, Supercritical water desalination (SCWD) of multi-component brines, *J. Supercrit. Fluids* 188 (2022) 105687, <https://doi.org/10.1016/j.supflu.2022.105687>.
- [22] C.Y. Ma, J.J. Liu, Y. Zhang, X.Z. Wang, Simulation for scale-up of a confined jet mixer for continuous hydrothermal flow synthesis of nanomaterials, *J. Supercrit. Fluids* 98 (2015) 211–221, <https://doi.org/10.1016/j.supflu.2014.12.016>.
- [23] Y. Zhang, S. Wang, Y. Li, J. Zhang, D. Xu, C. Yang, J. Yang, J. Li, T. Xu, Inorganic salts in sub-/supercritical water—Part A: behavior characteristics and mechanisms, *Desalination* 496 (2020) 114674, <https://doi.org/10.1016/j.desal.2020.114674>.
- [24] V.M. Valyashko, Heterogeneous fluids in supercritical binary and ternary water–salt systems, *Fluid Phase Equilibria* (2010).
- [25] A. Matayeva, A.S. Madsen, P. Biller, Evaluation of different fiber impurities on hydrothermal liquefaction of mixed textile waste, *Resour. Conserv. Recycl.* 190 (2023) 106833, <https://doi.org/10.1016/j.resconrec.2022.106833>.
- [26] A. Amrullah, Y. Matsumura, Supercritical water gasification of sewage sludge in continuous reactor, *Bioresour. Technol.* 249 (2018) 276–283, <https://doi.org/10.1016/j.biortech.2017.10.002>.
- [27] M. Magdeldin, M. Järvinen, Supercritical water gasification of Kraft black liquor: process design, analysis, pulp mill integration and economic evaluation, *Appl. Energy* 262 (2020) 114558, <https://doi.org/10.1016/j.apenergy.2020.114558>.
- [28] K. Ihara, H. Ueda, K. Sue, T. Nonaka, K. Arai, Decomposition of sodium thiosulfate and sodium thiocyanate in supercritical water, *J. Jpn. Inst. Energy* 85 (2006) 126–134, <https://doi.org/10.3775/jie.85.126>.
- [29] P.M. May, D. Batka, G. Hefter, E. Königsberger, D. Rowland, Goodbye to S<sup>2-</sup> in aqueous solution, *Chem. Commun.* 54 (2018) 1980–1983, <https://doi.org/10.1039/C8CC00187A>.
- [30] J. Reimer, F. Vogel, High pressure differential scanning calorimetry of the hydrothermal salt solutions K<sub>2</sub>SO<sub>4</sub>–Na<sub>2</sub>SO<sub>4</sub>–H<sub>2</sub>O and K<sub>2</sub>HPO<sub>4</sub>–H<sub>2</sub>O, *RSC Adv.* 3 (2013) 24503, <https://doi.org/10.1039/c3ra43725f>.
- [31] J. Reimer, F. Vogel, Influence of anions and cations on the phase behavior of ternary salt solutions studied by high pressure differential scanning calorimetry, *J. Supercrit. Fluids* 109 (2016) 141–147, <https://doi.org/10.1016/j.supflu.2015.10.018>.
- [32] V.M. Valyashko, Phase equilibria of water–salt systems at high temperatures and pressures, (n.d.) 45.
- [33] M. Schubert, J. Aubert, J.B. Müller, F. Vogel, Continuous salt precipitation and separation from supercritical water. Part 3: interesting effects in processing type 2 salt mixtures, *J. Supercrit. Fluids* 61 (2012) 44–54, <https://doi.org/10.1016/j.supflu.2011.08.011>.
- [34] M.M. DiPippo, K. Sako, J.W. Tester, Ternary phase equilibria for the sodium chloride–sodium sulfate–water system at 200 and 250 bar up to 400 °C, *Fluid Phase Equilibria* 157 (1999) 229–255, [https://doi.org/10.1016/S0378-3812\(99\)00039-4](https://doi.org/10.1016/S0378-3812(99)00039-4).
- [35] T. Voisin, A. Erriguible, C. Aymonier, Influence of multiphasic systems on salt(s) solubility in supercritical water: the case of NaCl and NaCl–Na<sub>2</sub>SO<sub>4</sub>, *J. Supercrit. Fluids* 152 (2019) 104567, <https://doi.org/10.1016/j.supflu.2019.104567>.
- [36] M. Schubert, J.W. Regler, F. Vogel, Continuous salt precipitation and separation from supercritical water. Part 2. Type 2 salts and mixtures of two salts, *J. Supercrit. Fluids* 52 (2010) 113–124, <https://doi.org/10.1016/j.supflu.2009.10.003>.
- [37] M. Schubert, J.B. Müller, F. Vogel, Continuous hydrothermal gasification of glycerol mixtures: effect of glycerol and its degradation products on the continuous salt separation and the enhancing effect of K<sub>3</sub>PO<sub>4</sub> on the glycerol degradation, *J. Supercrit. Fluids* 95 (2014) 364–372, <https://doi.org/10.1016/j.supflu.2014.09.011>.
- [38] J. Reimer, Biomass Related Salt Solutions at Hydrothermal Conditions, ETH Zur. (2015), <https://doi.org/10.3929/ethz-a-010578835>.
- [39] NIST Chemistry WebBook, NIST Standard Reference Database Number 69, n.d. (<http://webbook.nist.gov/chemistry/>).
- [40] S. Viereck, Experimental and numerical investigations of salt separation from biomass at hydrothermal conditions exploiting aqueous solutions of sodium sulfate and pure water as model systems, ETH Zur. (2018), <https://doi.org/10.3929/ETHZ-B-000270697>.
- [41] J. Reimer, G. Peng, S. Viereck, E. De Boni, J. Breinl, F. Vogel, A novel salt separator for the supercritical water gasification of biomass, *J. Supercrit. Fluids* 117 (2016) 113–121, <https://doi.org/10.1016/j.supflu.2016.06.009>.
- [42] D.A. Kulik, T. Wagner, S.V. Dmytrieva, G. Kosakowski, F.F. Hingerl, K. V. Chudnenko, U.R. Berner, GEM-Selektor geochemical modeling package: revised algorithm and GEMS3K numerical kernel for coupled simulation codes, *Comput. Geosci.* (2012), <https://doi.org/10.1007/s10596-012-9310-6>.
- [43] G.D. Miron, D.A. Kulik, Y. Yan, J. Tits, B. Lothenbach, Extensions of CASH+ thermodynamic solid solution model for the uptake of alkali metals and alkaline earth metals in C-S-H, *Cem. Concr. Res.* 152 (2022) 106667, <https://doi.org/10.1016/j.cemconres.2021.106667>.
- [44] M. Schubert, J.W. Regler, F. Vogel, Continuous salt precipitation and separation from supercritical water. Part 1: type 1 salts, *J. Supercrit. Fluids* 52 (2010) 99–112, <https://doi.org/10.1016/j.supflu.2009.10.002>.
- [45] G. Brunner, Corrosion in Hydrothermal and Supercritical Water, in: G. Brunner (Ed.), in: *Supercritical Fluid Science and Technology*, Elsevier, 2014, pp. 591–619.
- [46] G. Peng, Methane Production from Microalgae via Continuous Catalytic Supercritical Water Gasification: Development of Catalysts and Sulfur Removal Techniques, (n.d.) 238.
- [47] C. De Blasio, G. Lucca, K. Özdenkci, M. Mulas, K. Lundqvist, J. Koskinen, M. Santarelli, T. Westerlund, M. Järvinen, A study on supercritical water gasification of black liquor conducted in stainless steel and nickel-chromium-molybdenum reactors: a study on supercritical water gasification, *J. Chem. Technol. Biotechnol.* 91 (2016) 2664–2678, <https://doi.org/10.1002/jctb.4871>.
- [48] N. Boukis, W. Habicht, G. Franz, E. Dinjus, Behavior of Ni-base alloy 625 in methanol-supercritical water systems, *Mater. Corros.* 54 (2003) 326–330, <https://doi.org/10.1002/maco.200390072>.
- [49] R. Fujisawa, M. Sakai, Y. Kurata, Y. Watanabe, Corrosion behaviour of nickel base alloys and 316 stainless steel in supercritical water under alkaline conditions, *Corros. Eng. Sci. Technol.* 40 (2005) 244–248, <https://doi.org/10.1179/174327805x66308>.
- [50] K. Khumsa-Ang, M. Edwards, S. Rousseau, General corrosion of chromium-coated zirconium- and titanium-based alloys in supercritical water at 500 °C, *J. Nucl. Eng. Radiat. Sci.* 6 (2020) 031102, <https://doi.org/10.1115/1.4045387>.
- [51] S. Li, T. Deng, Y. Zhang, Y. Liang, R. Li, T. Dong, Review on the creep resistance of high-temperature titanium alloy, *Trans. Indian Inst. Met.* 74 (2021) 215–222, <https://doi.org/10.1007/s12666-020-02137-x>.
- [52] H. Tran, X. Mao, J. Cameron, C.M. Bair, Autocauticizing of Smelt with Sodium Borates, (1999).
- [53] S.H. Kochesfahani, C.M. Bair, M. Kirk, Partial Borate Autocauticizing: A New Technology in Chemical Recovery, 59 (2006) 6.

- [54] J. Janson, The use of unconventional alkali in cooking and bleaching. 5. Autocausticizing reactions, *Pap. ja puu* 60 (1979) 20–24.
- [55] M. Naqvi, J. Yan, E. Dahlquist, Synthetic gas production from dry black liquor gasification process using direct causticization with CO<sub>2</sub> capture, *Appl. Energy* 97 (2012) 49–55, <https://doi.org/10.1016/j.apenergy.2011.11.082>.
- [56] M. Naqvi, J. Yan, E. Dahlquist, Bio-refinery system in a pulp mill for methanol production with comparison of pressurized black liquor gasification and dry gasification using direct causticization, *Appl. Energy* 90 (2012) 24–31, <https://doi.org/10.1016/j.apenergy.2010.12.074>.
- [57] M. Naqvi, J. Yan, E. Dahlquist, Energy conversion performance of black liquor gasification to hydrogen production using direct causticization with CO<sub>2</sub> capture, *Bioresour. Technol.* 110 (2012) 637–644, <https://doi.org/10.1016/j.biortech.2012.01.070>.
- [58] B. Segal, The causticization of sodium sulphate, *S. Afr. J. Chem.* 8 (1925) 11–15.
- [59] I. Nohlgren, K. Magnusson, T. Richards, Recycling effects in the titanate direct causticization process, *Nord. Pulp Pap. Res. J.* 20 (2005) 298–303.
- [60] I. Nohlgren, Non-conventional causticization technology: a review, *Nord. Pulp Pap. Res. J.* 19 (2004) 470–480.
- [61] H. Tran, E.K. Vakkilainen, The kraft chemical recovery process, *Tappi Kraft Pulping Short. Course* (2008) 8.
- [62] H. Wang, J. Zeuschner, M. Eremets, I. Troyan, J. Willams, Stable solid and aqueous H<sub>2</sub>CO<sub>3</sub> from CO<sub>2</sub> and H<sub>2</sub>O at high pressure and high temperature, *Sci. Rep.* 6 (2016) 19902, <https://doi.org/10.1038/srep19902>.